Analyses of Coherent Lidar Wind Measurement Missions

Contract No. NAS8-38609

Delivery Order No. 128

Contract Period 11/02/94 - 11/01/95

Report Date 8/28/96

Gary D. Spiers
Center for Applied Optics
University of Alabama in Huntsville
Huntsville
AL 35899
(205) 890 6030 ext. 420

Table of Contents

Introduction

This report details work carried out under NASA contract NAS8-38609 delivery order no. 128.

Much of the work undertaken involved additions to the coherent lidar model, including the addition of performance as a function of altitude (Chapter 1. and Appendix I), a receiver design section (Chapter 2. and Appendix III), the development of a simple orbit model Appendix II) suitable for use in plotting orbits, swath and shot patterns and estimating power availability (Appendix IV) and the inclusion of Fascode derived atmospheric extinction (Chapter 3.).

Considerable time was occupied with assisting NASA MSFC in the design and analysis of lidar instruments, both for the AEOLUS conceptual designs within MSFC (one such analysis is included in Appendix IV) and of proposed NASA MSFC instruments for the New Millennium Program.

Chapter 1. Coherent lidar performance as a function of altitude

The minimum detectable backscatter level for a coherent Doppler lidar instrument is a function of the range to the target and of the optical properties of the atmosphere between the lidar and target. The space-based coherent lidar model developed previously was modified to permit the calculation of the minimum detectable backscatter as a function of altitude. Figure (1-1) shows a representative output plot. It should be noted that typically backscatter vs. altitude plots have the altitude on the y-axis as this is more intuitive however, limitations of the plotting facilities within the programming package prevent placing the independent variable (altitude) on the y-axis and the dependent variable (backscatter) on the x-axis. This disadvantage is offset by the ability to easily cut and paste the calculated results from the model into a presentation quality graphics package when necessary.

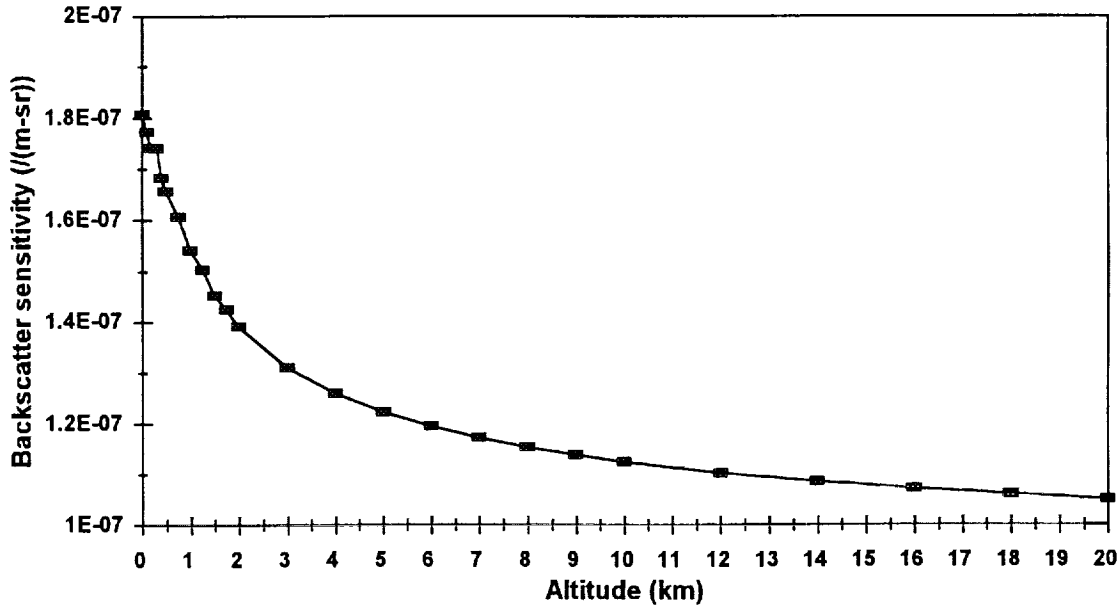

Figure (1-1) A representative backscatter sensitivity as a function of altitude plot.

It can be seen from the figure that the altitude interval between data points increases at higher altitudes - this was implemented to speed up calculation of results. Close to the earth's surface, the atmospheric extinction varies considerably as a function of altitude and this will affect the backscatter sensitivity so the data points are calculated frequently (100 m vertical separation). Table (1.1) lists the altitude ranges at which the various step sizes are used. It should be noted that these steps represent the points at which the backscatter sensitivity is calculated and not the step size for calculation of the atmospheric extinction. For each backscatter sensitivity calculation point the

atmospheric extinction to that altitude is calculated using the full resolution of the model (100 m in the vertical over the complete altitude range).

Altitude Range (m)	Altitude step (m)
$z \leq 500$	100
$500 < z \leq 2000$	250
$2000 < z \leq 8000$	1000
$8000 < z \leq 19999$	2000

Table (1.1) Step sizes used for calculation of the backscatter sensitivity as a function of altitude (see text).

The code for this task is listed in Appendix I.

Chapter 2. Receiver Design

2.1 The Doppler shift problem

A concern in the design of a suitable receiver for a space based coherent lidar, such as the AEOLUS[1],[4] instrument design studied at NASA MSFC, is that the instrument will probably employ some form of scan geometry[2] and will consequently see an azimuth angle dependent Doppler shift due to components of the spacecraft velocity and earth rotational velocity. The spacecraft induced Doppler shift is the major component and is simply given by:

$$\delta f(\lambda, h, z, \varphi_n, \varphi_{az}) = \frac{2}{\lambda} vsat(h) \sin(nadalt(h, \varphi_n, z)) \cos(\varphi_{az}) \quad (2\text{-}1)$$

where λ is the operating wavelength, h is the instrument orbit height, z is the target altitude, φ_n is the instrument nadir angle and φ_{az} is the instrument azimuth angle relative to the satellite velocity vector (Figure (2-1)). As a consequence of the earth's curvature, the nadir angle at the target is

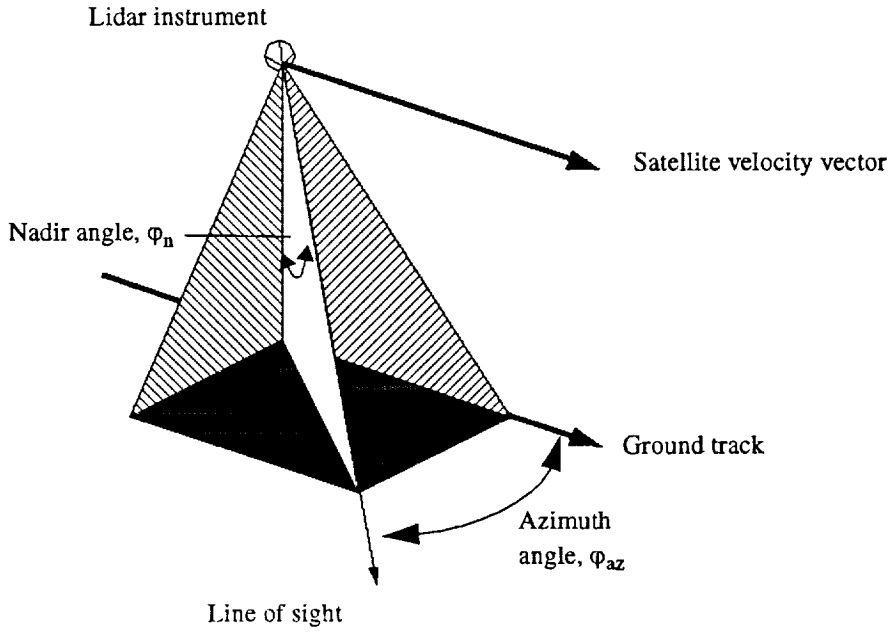

Figure (2-1) The geometry of the satellite velocity vector, ground track vector, instrument line-of-sight, nadir and azimuth angles.

slightly larger than the nadir angle at the instrument and the function nadalt(h,φ_n,z) in equation (2-1) determines the target nadir angle (assuming a spherical earth) by:

$$nadalt(h, \varphi_n, z) = \operatorname{asin}\left[(h + r_e) \frac{\sin(\varphi_n)}{(r_e + z)} \right] \quad (2\text{-}2)$$

where r_e is the radius of the earth. Table (2.1) shows both the actual value of nadalt(h,φ_n,z) and the percentage error in $\delta f(\lambda,h,z,\varphi_n,\varphi_{az})$ that would occur if the change in nadir angle due to the earth's curvature was not accounted for. The table shows these values for a target altitude of 0 m and several values of spacecraft altitude and nadir angle.,

Nadir, (deg.)	Altitude, (km)		
	350	525	825
30	31.9	32.9	34.9
40	42.8	44.3	46.9
50	54.1	56.4	60.5

a)

Altitude, (km)		
350	525	825
5.5 %	8.0 %	12.0 %
5.5 %	8.0 %	12.0 %
5.5 %	8.0 %	12.0 %

b)

Table (2.1) a) Actual nadir angle at the ground when the change in nadir angle due to the earth's curvature is accounted for and b) the percentage error introduced into the spacecraft induced frequency shift when this effect is not considered.

The Doppler shift due to the earth's rotational velocity is a function of both the latitude of the spacecraft and the azimuth angle. The earth's rotational velocity at any latitude is simply given by:

$$V_e(\text{lat}) = V_{eq}\cos(\text{lat}) \tag{2-3}$$

where Veq is the earth's rotational velocity at the equator and lat is the latitude of interest. Appendix II shows an orbit calculation and plot in which the change in the angle between the spacecraft velocity vector and the lines of longitude and latitude as a function of latitude can clearly be seen. For every latitude there is some azimuth angle at which the full Doppler shift due to the earth's rotation will be seen. As the maximum value of this shift occurs at the equator, all the plots shown here assume the spacecraft orbit is crossing the equator as this introduces the maximum perturbation due to the earth's rotational velocity. Any design that accommodate this maximum value will be able to accommodate smaller frequency shifts at other latitudes. The two micron wavelength region currently being studied for an operational space based lidar instrument means that this varying Doppler shift will be large. Figure (2-2) shows this Doppler shift as a function of azimuth angle for a two micron instrument with a 30 deg. nadir angle and a 350 km high orbit. The dotted straight lines represent the bandwidth (~1.3 GHz) of commercially available InGaAs detectors. It is obvious that the bandwidth of the detector is insufficient to cover the bandwidth of the signal.

2.2 Conceptual design of the optical portion of the receiver

To overcome this, the gross Doppler shift due to the component of the spacecraft velocity can be removed by using a frequency tunable local oscillator. An idealised frequency tuning curve for such a local oscillator is also shown in Figure (2-2) together with the residual frequency shift seen by the detector - the frequency shift for both positive and negative maximum horizontal wind velocities (± 100 m/s for the case considered here). Present in the residual frequency shift is the

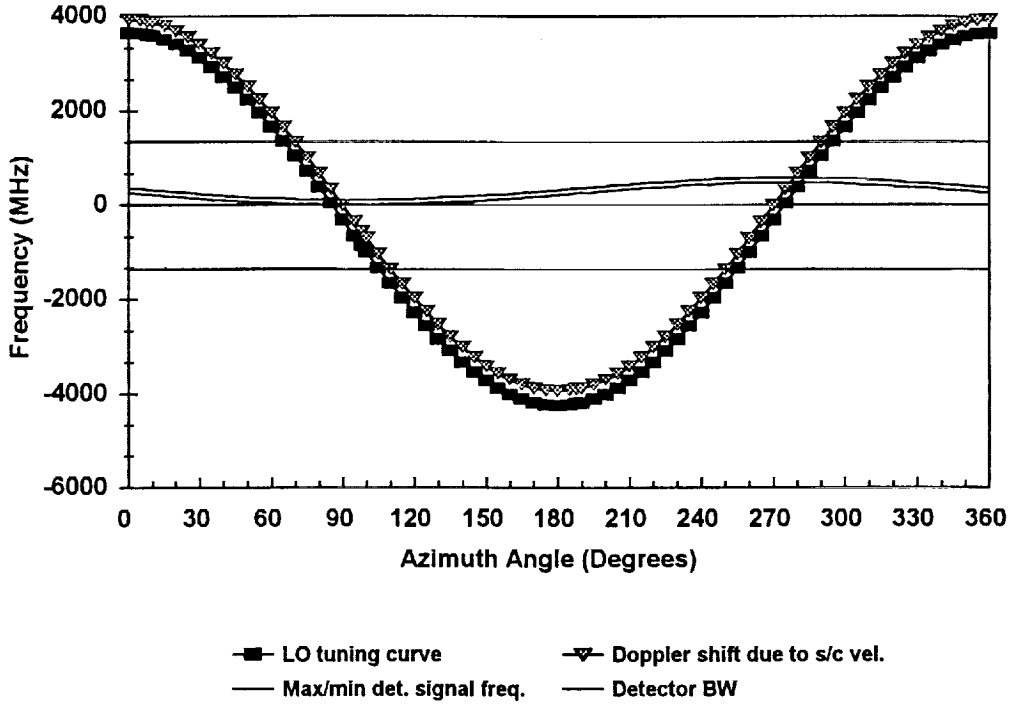

Figure (2-2) Doppler frequency shifts due to the component of the spacecraft velocity seen by the satellite, typical detector bandwidths, an idealised local oscillator tuning range and the resultant signal bandwidth as a function of telescope azimuth angle.
component of the earth's rotation which causes the center frequency to vary as a function of azimuth angle as discussed previously.

If a tunable local oscillator is used there must be some scheme to ensure that the frequency difference between the local oscillator and the pulsed laser is known. Figure (2-3) shows one possible scheme in which a master oscillator is frequency locked against a reference, such as a Fabry-Perot cavity. The figure also shows the various optical frequencies, f_x at different portions of the receiver where the subscript x is either mo, lo or t which represent the master oscillator, local oscillator and pulsed transmitter laser respectively. The frequency is also potentially a function of time and $f_x(t1)$ represents the time of the outgoing (transmitted) pulse and $f_x(t2)$ represents the returning signal pulse a few milliseconds later. The object to be measured, the Doppler shift induced on the signal due to the spacecraft velocity, earth's rotational velocity and the atmospheric wind velocity is δf_T. The output from the master oscillator is then used for three purposes:

1.) to control the output frequency of the pulsed laser by injection seeding.

2.) as a local oscillator for heterodyning against the output from the pulsed laser. This verifies the frequency of the pulsed transmitter laser is correct and also measures the spectrum of the pulsed laser.

3.) as a local oscillator for heterodyning against the output of the tunable local oscillator so that the tunable oscillator offset from the transmitter laser can be correctly determined. The heterodyne beat frequencies $f_A(t1)$, $f_B(t2)$ and $f_C(t2)$ on each of the detectors A, B and C respectively are given by:

$$f_A(t1) = f_t(t1) - f_{mo}(t1) \tag{2-4}$$

$$f_B(t2) = f_{mo}(t2) - f_{lo}(t2) \tag{2-5}$$

and

$$f_C(t2) = f_t(t1) + \delta f_T - f_{lo}(t2) \tag{2-6}$$

Combining these we obtain:

$$\delta f_T = f_C(t2) + f_{mo}(t2) - f_B(t2) - f_A(t1) - f_{mo}(t1) \tag{2-7}$$

which expresses the Doppler shift frequency in terms of the measured heterodyne frequencies and the master oscillator frequency. Provided that over the round trip time of the signal (~3 ms @ 350 km altitude, 30 deg nadir angle) the master oscillator frequency is stable then the master oscillator frequencies in equation (2-7) cancel and we are left with an expression that contains only measurable parameters.

2.3 Conceptual design of the electronic portion of the receiver

The electronics design concept discussed here was originally sketched out by Mr. Steve Johnson of the NASA Marshall Space Flight Center.

The function of the electronics portion of the receiver, shown in block form in Figure (2-4) is to reduce the bandwidth of the signal as much as possible so that it can be readily digitised and stored efficiently. Figure (2-5)A shows the frequencies out of the optical detector after the optical heterodyne mixing has removed the gross Doppler shift due to the spacecraft velocity. It can be seen that the magnitude of the frequency shift due to the Doppler shift from the component of the earth's rotational velocity is large compared to the wind signal. In order to reduce the A/D bandwidth requirements to a minimum, the signal is further mixed with a frequency synthesised local oscillator in the electronics of the receiver. Figure (2-5)B shows the frequency tuning required from this local oscillator as a function of azimuth angle and Figure (2-5)C shows the signal after mixing with this electronic local oscillator. It can be seen that the frequency of the signal is now independent of the azimuth angel, i.e. all the frequency perturbation effects have been removed. The only remaining task is to split the signal into I and Q components and digitise it. Figure (2-5)D shows the frequency bandwidths required at various points through the electronics design.

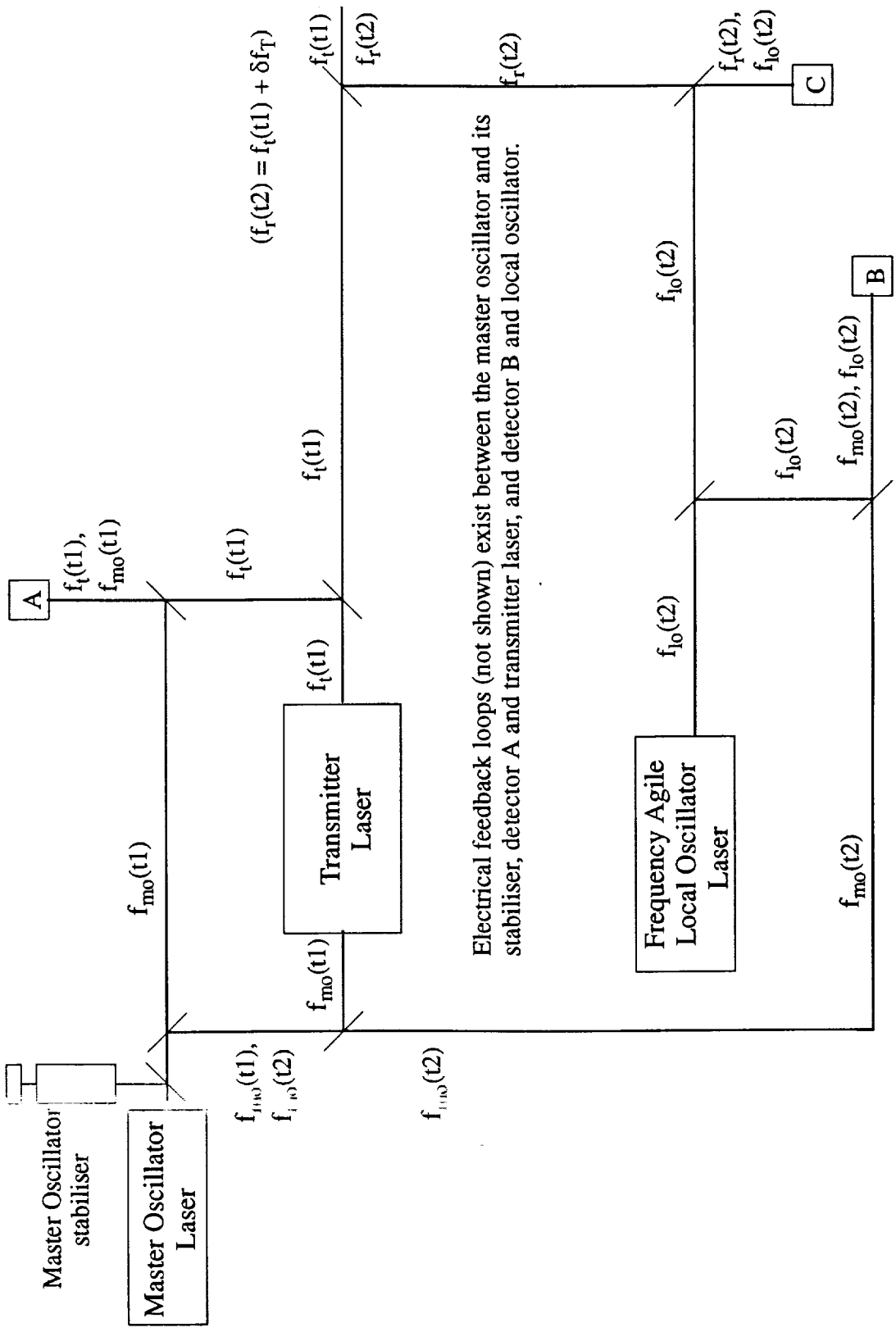

Figure (2-3) Schematic showing frequency relationships between components of the optical portion of the receiver.

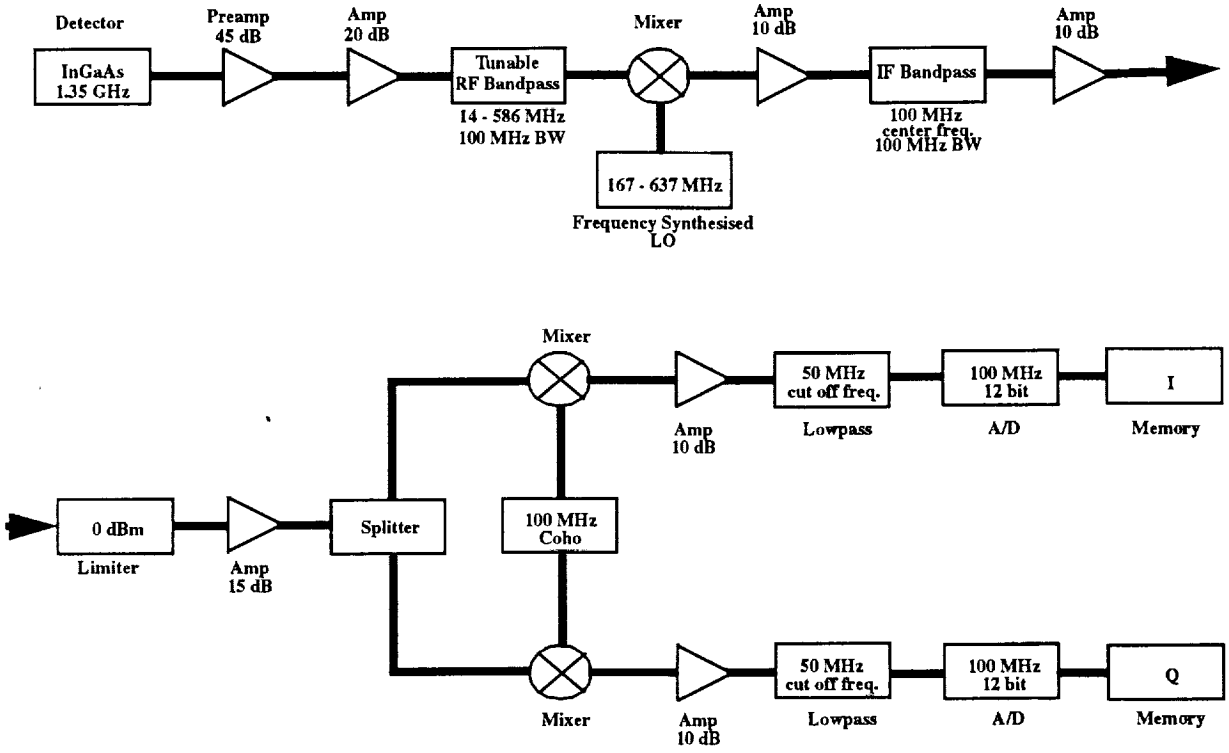

Figure (2-4) Block diagram of the electronic portion of the receiver.

2.3.1 Optical detector shot noise performance

In order for the optical heterodyne detection system to work, the noise on the detector must be dominated by the local oscillator shot noise. The two major noise contributors are the shot noise and the Johnson noise in the detector. The noise on the detector is given by:

$$N = \frac{2e^2\eta P_{LO}B_S}{h\upsilon} + \frac{4kT_eB_S}{R_e} \quad \text{where} \tag{2-8}$$

$$\frac{1}{R_e} = 2\pi B_D C \tag{2-9}$$

$$N = \frac{2e^2\eta P_{LO}B_S}{h\upsilon} + 8\pi kT_eB_DCB_S \tag{2-10}$$

where e, η, P_{LO}, B_S, h, ν, k, T_e, R_e, B_D and C are the charge on an electron, detector quantum efficiency, local oscillator power, search bandwidth, Planck's constant, LO frequency, Boltzman constant, equivalent detector temperature and resistance, detector bandwidth and detector capacitance respectively. shows the noise characteristics for a detector with 3 pF of capacitance[3], an operat-

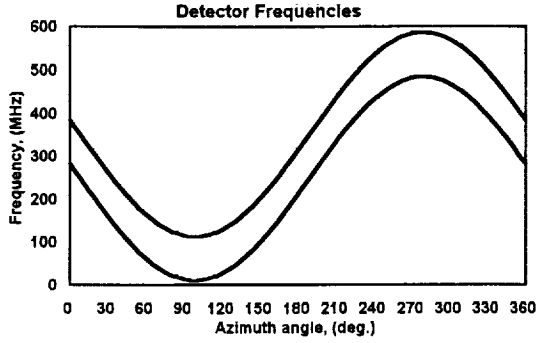

A) Frequencies at the detector output.

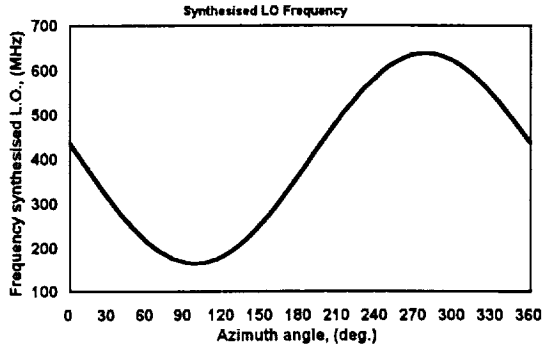

B) Tuning curve of the electronic local oscillator.

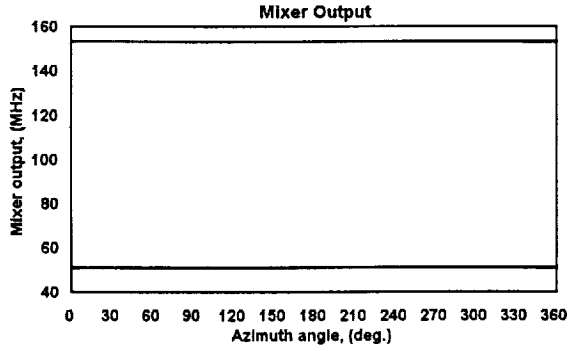

C) Output from the mixer.

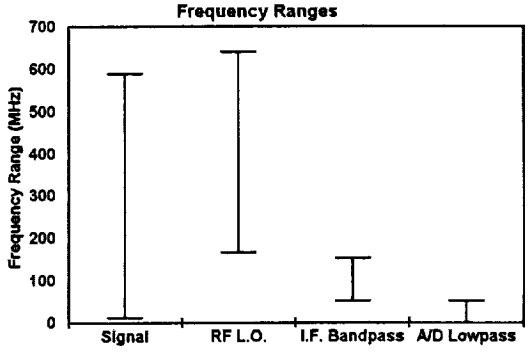

D) Bandwidths required in the receiver.

Figure (2-5) A series of plots showing frequencies at various points within the receiver.

ing temperature of 300 K and a local oscillator power of 1.5 mW. It can be seen that the shot noise dominates the detector noise characteristics out to ~1.5 GHz.

2.3.2 Data Rates

Figure (2-7) shows a summary of the data requirements from the design, it includes the effect of:

1.) nadir pointing errors - if there is an error in the nadir angle then it will have two effects on the data requirement. If the nadir angle becomes larger (smaller) then the line of sight component of the horizontal wind velocity becomes larger (smaller) and a larger (smaller) A/D rate than that required for the ideal case is needed. In conjunction with this the path length through the atmosphere will become longer (shorter) for an increase (decrease) in the nadir angle.

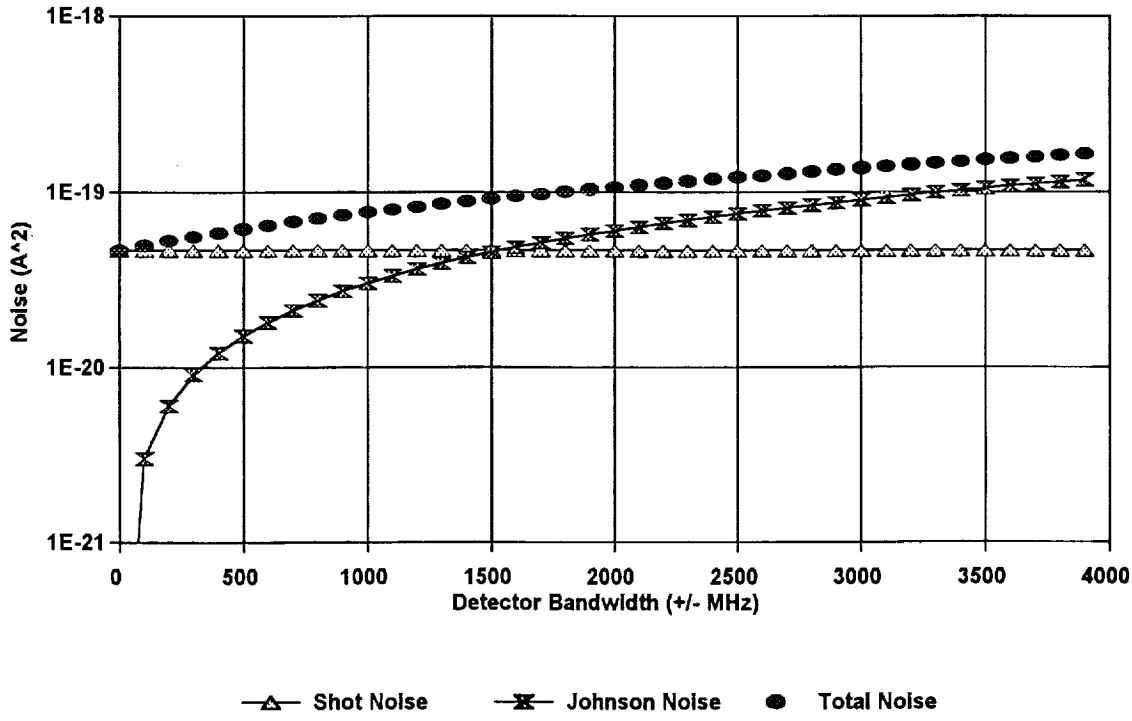

Figure (2-6) Detector noise characteristics for C = 3 pF, T_e = 300 K and P_{LO} = 1.5 mW.

2.) transmitter/local-oscillator offset errors - the frequency offset between the transmitted pulse can not be absolutely controlled. The data sampling must be designed to accommodate the size of any likely frequency offset error that may arise.

3.) sampling above the Nyquist criteria - most lidar data collection schemes generally sample the data at a rate slightly faster than that determined by the Nyquist criteria.

4.) the number of bits per sample.

5.) the maximum and minimum altitudes from which data is to be collected and the 'guard' region around this sample - the maximum and minimum altitudes are determined by the science requirements and sensitivity of the instrument. The guard region is additional data collected on either side of the data sample to ensure that no data is missed.

6.) the number of ancillary words per pulse - in order to correctly assign the collected data to a three dimensional location in the earth's atmosphere additional satellite position and pointing information must be stored with each sample. Other data such as instrument calibration information may also be required to reconstruct and calibrate the data correctly.

Wavelength	2.065479	µm					
Max. horizontal velocity	100	m/s					
Max. line of sight velocity (occurs at ground)	52.7466857	m/s					
Max. nadir error (any direction)	+/- 0.1	deg.					
Worst case line of sight velocity shift due to nadir error	12.4379616	m/s					
Max line of sight velocity allowing for nadir error	65.1846473	m/s					
Velocity bandwidth required to this point	130.369295	m/s					
Signal bandwidth required to this point	126.236379	MHz					
XMTR/LO frequency offset error	+/- 5	MHz					
Additional bandwidth to account for XMTR/LO offset error	10	MHz					
Total bandwidth required	136.236379	MHz					
Real/Complex receiver geometry	Complex						
Sampling rate over Nyquist	1.1	(1 = Nyquist, 2 = Twice as many samples as Nyquist etc.)					
Sampling rate required/ channel	149.860017	Msamples/s					
No. bits	12	bits/sample					
pk. bits/s (one channel)	1.7983E+09	bits/s					
pk. bits/s (all channels)	3.5966E+09	bits/s		No Error		With Error	
Max altitude	15	km	nadir	31.7509	deg.	31.85814	de
Min altitude	0	km	nadir	31.8345	deg.	31.942	de
slant range margin	1	km					
slant range	18.6478888	km					
digitisation time	124.405323	µs					
bits/pulse	447442	bits/pulse					
ancillary words/ pulse	20	words/pulse					
total bits/pulse	447682	bits/pulse					
PRF	20	Hz					
Bits/s averaged over one second	8953640	bits/s					
Orbit duration	5481.50413	s					
Data storage	4.9079E+10	bits/orbit					

Figure (2-7) Data requirement summary

7.) instrument pulse repetition rate - determines the number of shots and hence total number of samples collected in a given time.

2.4 Description of the numerical model developed

A Quattro Pro spreadsheet (Appendix III) was developed to assist analysis of the receiver design. The spread sheet dynamically takes parameters from the previously developed space based coherent lidar model and together with some additional inputs from the user calculates and displays a conceptual receiver design. Constraints built into the model permit it to automatically adjust to correct for changes in the input variables. The goal of the model is to generate a design in which the A/D sample rate is minimised. The model is sumarised over five spreadsheet notebook pages, each of which is shown in Appendix III.

The first page displays the main parameters of the model together with a plot of the optical frequencies and detector bandwidths. The second page displays a block diagram of the electronic portion of the receiver together with key frequencies at various locations throughout the receiver. Also on this page are 'buttons' to perform a recalculation of the page and to display full-screen plots of frequency vs. azimuth angle at various key locations in the design. The third page displays a plot of the detector noise characteristics. The fourth consists of smaller summary plots of all the plots available on the second page and finally the fifth page consists of a data analysis page for determining the data rate and storage requirements of a given instrument. This data analysis

includes the effects of various errors in that receiver and instrument sub systems that may lead to an increase in the data requirement.

2.5 Discussion

In the example here it has been assumed that the mean frequency of the local oscillator is offset from the frequency of the transmitted pulse by 300 MHz. The use of this offset avoids any ambiguity in the signal and. Figure (2-8) shows the resultant frequencies when no offset between the

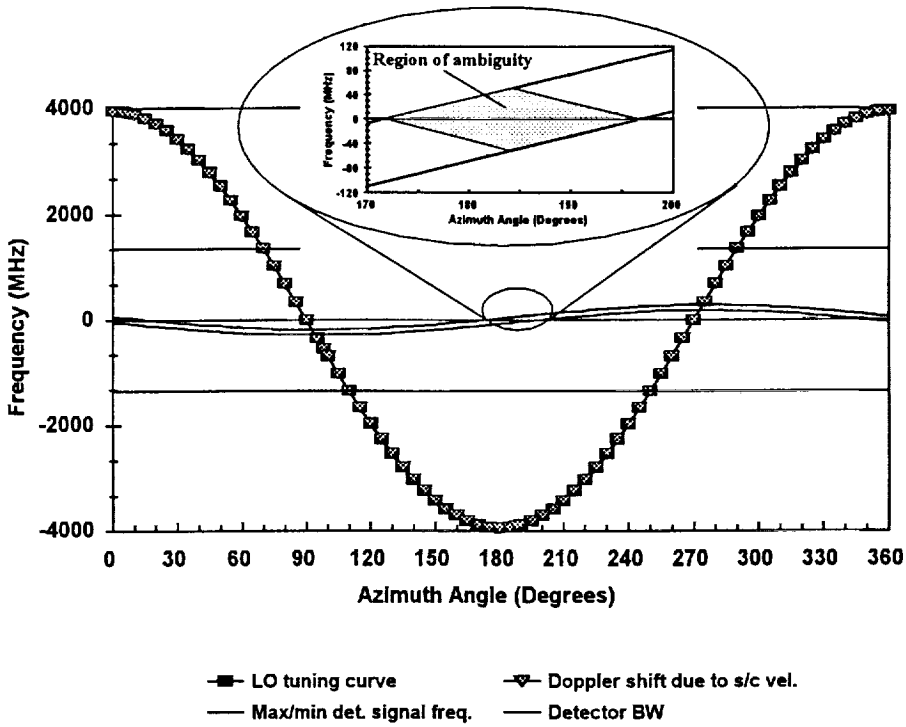

Figure (2-8) As Figure (2-2) but without an offset frequency between the local oscillator and transmitter frequencies.

local oscillator and transmitter laser exists. The highlighted region between ~170 and ~200 degrees together with a similar region between ~350 and ~380 degrees are areas where a frequency can represent two different wind velocities depending on the sign of the frequency. The sign of the frequency can not be determined from the detected signal and so an ambiguity in determining the wind velocity arises.

From Figure (2-2) it can be seen that after the local oscillator has removed the gross Doppler shift due to the spacecraft's velocity the signal frequency varies from ~14 MHz to ~600 MHz which is comfortably within the bandwidth of the detector. The only problem with this scheme is that the local oscillator is now required to tune ±3.95 GHz about a frequency offset 300 MHz from line center of the transmitter frequency. In addition to the tuning requirement, the frequency error in the local oscillator should be less than ~ 1 MHz in order to achieve a velocity measurement accuracy of ~ 1 m/s or less for the whole instrument. This combination of requirements puts severe

demands on the local oscillator design and performance. One possible method of relieving these demands is to adjust the local oscillator tuning so that full advantage is taken of the detector bandwidth. Figure (2-9) shows a scheme which minimises the tuning requirements of the local oscilla-

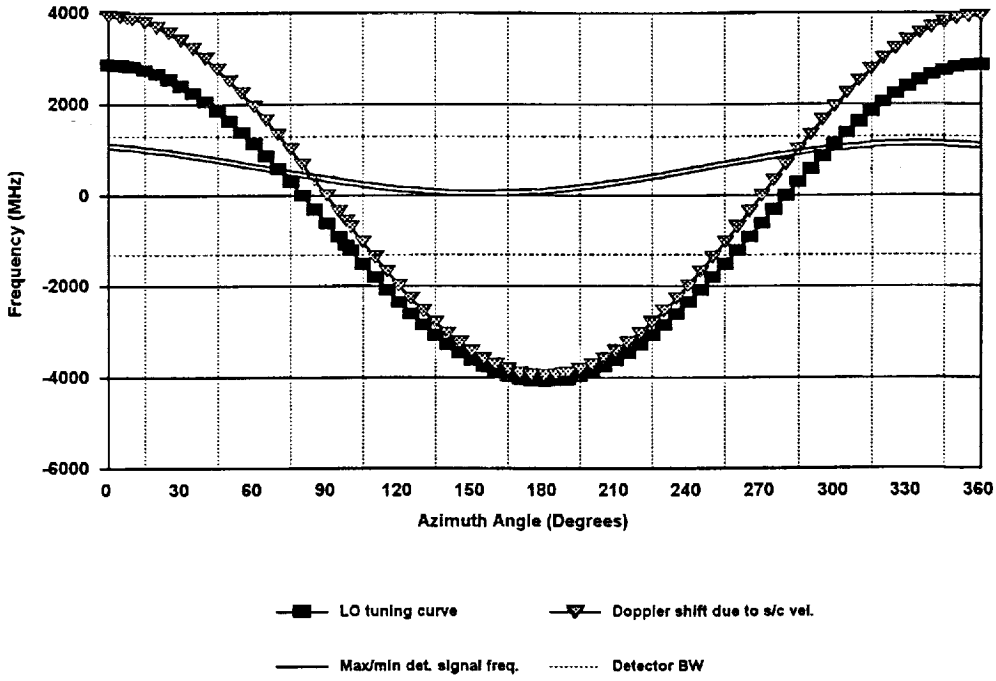

Figure (2-9) Optimised local oscillator offset and tuning range to maximise use of the detector bandwidth while minimising the local oscillator tuning range.

tor by maximising the use of the detector bandwidth. Note that in order to make full use of the detector bandwidth, the local oscillator offset from the transmitter frequency has been increased to 600 MHz. Table (2.2) summarises the tuning requirements of the local oscillator for the two

Goal	Center Frequency Offset from Transmitter	Local Oscillator Tuning Range	Maximum Offset of Local Oscillator from Transmitter
Minimise detector bandwidth requirement.	300 MHz	7950 MHz	4275 MHz
Maximise use of detector bandwidth and minimise local oscillator tuning requirement.	600 MHz	6950 MHz	4075 MHz

Table (2.2) Tuning options summary for a detector bandwidth of 1.3 GHz.

schemes. It can be seen that for the detector bandwidth (1.3 GHz) considered, the active tuning

range of the local oscillator has been reduced by ~ 1 GHz compared to the scheme that simply tunes the local oscillator over the Doppler frequency shift range due to the satellite velocity offset. Unfortunately the maximum offset of the local oscillator from the transmitter center frequency is only reduced by 200 MHz from 4275 MHZ to 4075 MHz. At the time of writing this report, a local oscillator capable of demonstrating these characteristics had not been demonstrated.

Chapter 3. Other Activities

3.1 Atmospheric Extinction

The Fascode atmospheric extinction code was made operational for use with the lidar modeling program. Representative plots of extinction per km at ground level for a mid-latitude summer atmospheric model with no aerosol extinction are shown in Figure (3-1).

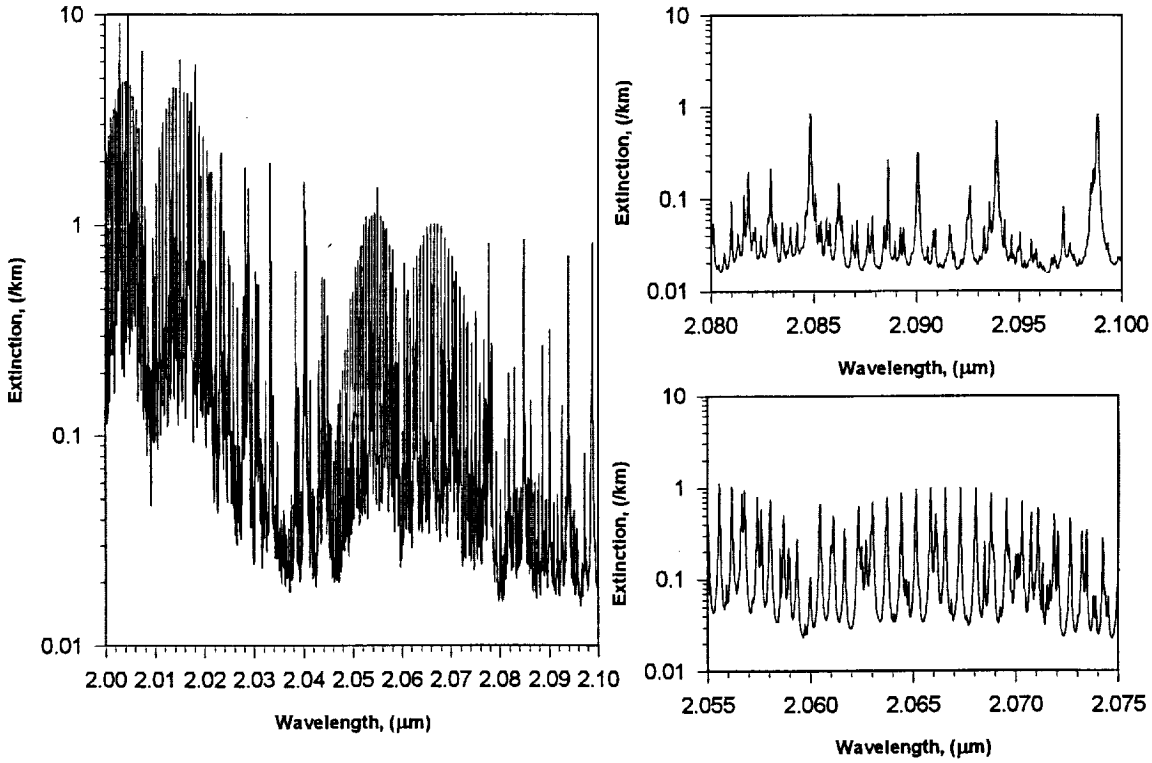

Figure (3-1) Representative plots of the output from the Fascode atmospheric extinction code.

3.2 NASA's New Millennium Program

A series of performance analyses for both 200 mJ, 50 cm and 25 mJ, 25 cm 2 μm coherent Doppler lidar instruments was performed for NASA MSFC in support of NASA's New Millennium Program. The instruments were similar to those developed under the AEOLUS[4] program at MSFC.

3.3 Meetings and Conferences

A paper on the receiver design was presented at the OSA Topical Meeting on Coherent Laser Radar[5] and a presentation was made on the New Millennium Program to the NOAA Working Group on space-based lidar winds.[6]

Chapter 4. References

[1] Kavaya,M.J., G.D. Spiers, E.S. Lobl, J. Rothermel and V.W. Keller; "Direct global measurements of tropospheric winds employing a simplified coherent laser radar using fully scalable technology and technique", Proc. SPIE:- Space Instrumentation and Dual-Use Technologies, **2214**, 237 - 249 (1994).

[2] See for example: Spiers, G.D.; "Lidar Performance Analysis", Final Report NASA Contract No. NAS8-38609, Delivery Order No. 57 (1994).

[3] Detector capacitance and local oscillator power data was provided by Dr. Farzin Amzajerdian of the Center for Applied Optics, University of Alabama in Huntsville.

[4] Spiers, G.D., "Lidar Analyses", Final Report NASA Contract No. NAS8-38609, Delivery Order No. 79 (1995).

[5] Spiers, G. D., F. Amzajerdian, and S.C. Johnson, "Design Considerations for a space based coherent Doppler lidar operating in the two micron wavelength region", in Coherent Laser Radar, Vol. 19, 1995 OSA Technical Digest Series (Optical Society of America, Washington DC, 1995), pp. 58-61.

[6] Spiers, G.D., "Enabling Technology for Space Based Laser Measurement of Winds: Free-Flyer Approach", in Minutes of the NOAA Working Group on Space-Based Lidar Winds, pp. 44-49 (July 1995).

Appendix I Performance vs. Altitude Code

The code listed here follows the same conventions as listed in previous reports ()and builds upon that code. The following table is a coded Quattro Pro macro to backsolve for the backscatter at which the probability of a good estimate is equal to 50%. It calls sections of code used in previous reports.

	A	B
4	step_no	26
5	altitude	19999
6		
7	betavalt	{FOR step_no,1,25,1,loop}
8		
9	loop	{CALC}
10		{LET +"A"&@STRING(step_no+15,0), altitude/1000}
11		{LET [lidar]alt,altitude}
12		{[lidar]50%BETA_CALC}
13		{CALC}
14		{LET +"B"&@STRING(step_no+15,0), [lidar]BETA}

Cell B5 calculates the altitude from the value of step_no using the following Quattro Pro formula:

@IF(step_no<7,(step_no-1)*100,@IF(step_no<13,(500+(step_no-6)*250),@IF(step_no<21,2000+(step_no-12)*1000,@IF(step_no<25,(step_no-20)*2000+10000,19999))))

This expression simply implements the step sizes outlined in Table (1.1).

Appendix II Orbit Calculation

The Mathcad document on the following pages calculates and displays orbit plots for the purpose of determining lidar instrument swath widths, repeat cycles, shot patterns and power budgets. It is not intended to rperesent a detailed orbit analysis.

This mathcad document calculates a simple circular orbit by calculating the angular position in the orbit as a function of time and then translates the co-ordinates of the satellite by rotation about the axes to get latitude, longitude position relative to the earth rotating beneath the spacecraft. It is only intended to provide a conceptual view of orbits.

Set up assorted constants

$G := 6.6725910^{-11} \cdot \frac{m^3}{kg \cdot sec^2}$ Gravitational constant $\quad r_e := 6371.315km$ Radius of earth

$\tau_e := 8.6399881 0^4 \cdot sec$ Average solar day (24 hrs) $\quad M_e := 5.979\,10^{24} \cdot kg$ Mass of earth

Variables

Orbit height $h := 350km$ Orbit Inclination $orbinc := 98 \cdot deg$ No. of orbits to plot $n := 5$

Calculate basic orbit parameters

Satellite velocity $V := \sqrt{\frac{GM_e}{(h + r_e)}}$ Time for one orbit $\tau_{orbit} := \frac{2 \cdot \pi \cdot (h + r_e)}{V}$

For the orbit selected above we have:

$V = 7.704\,10^3 \cdot m \cdot sec^{-1}$ and $\tau_{orbit} = 91.358 \cdot min$

Now calculate the basic circular orbit, allowing 5 sec between points.

$npts := ceil\left[\frac{\frac{\tau_{orbit}}{sec} \cdot n}{5}\right]$ $\quad i := 0..npts$ $\quad t_i := i \cdot 5 \cdot sec$ $\quad alpha_i := -\frac{t_i \cdot 2 \cdot \pi}{\tau_{orbit}}$

Change to x, y, z co-ordinates

$x_i := r_e \cdot \sin(90 \cdot deg) \cdot \cos(alpha_i)$ $\quad y_i := r_e \cdot \sin(90 \cdot deg) \cdot \sin(alpha_i)$ $\quad z_i := r_e \cdot \cos(90 \cdot deg)$

Rotate about x-axis by -orbinc degrees

$rotangle := -orbinc$ $\quad x1_i := x_i$ $\quad y1_i := y_i \cdot \cos(rotangle) + z_i \cdot \sin(rotangle)$ $\quad z1_i := y_i \cdot (-\sin(rotangle)) + z_i \cdot \cos(rotangle)$

Rotate about z to account for earths rotation

$longrot_i := mod\left(\frac{360 deg \cdot t_i}{60 \cdot 60 \cdot 24 \cdot sec}, 360 deg\right)$

$x2_i := x1_i \cdot \cos(longrot_i) + y1_i \cdot \sin(longrot_i)$ $\quad y2_i := -(x1_i \cdot \sin(longrot_i)) + y1_i \cdot \cos(longrot_i)$ $\quad z2_i := z1_i$

Change from x,y,z to long, lat, alt

$long_i := angle(x2_i, y2_i) - \pi$ $\quad lat_i := acos\left[\frac{z2_i}{\sqrt{(x2_i)^2 + (y2_i)^2 + (z2_i)^2}}\right] - \frac{\pi}{2}$ $\quad r3_i := \sqrt{(x2_i)^2 + (y2_i)^2 + (z2_i)^2}$

Plot Orbit

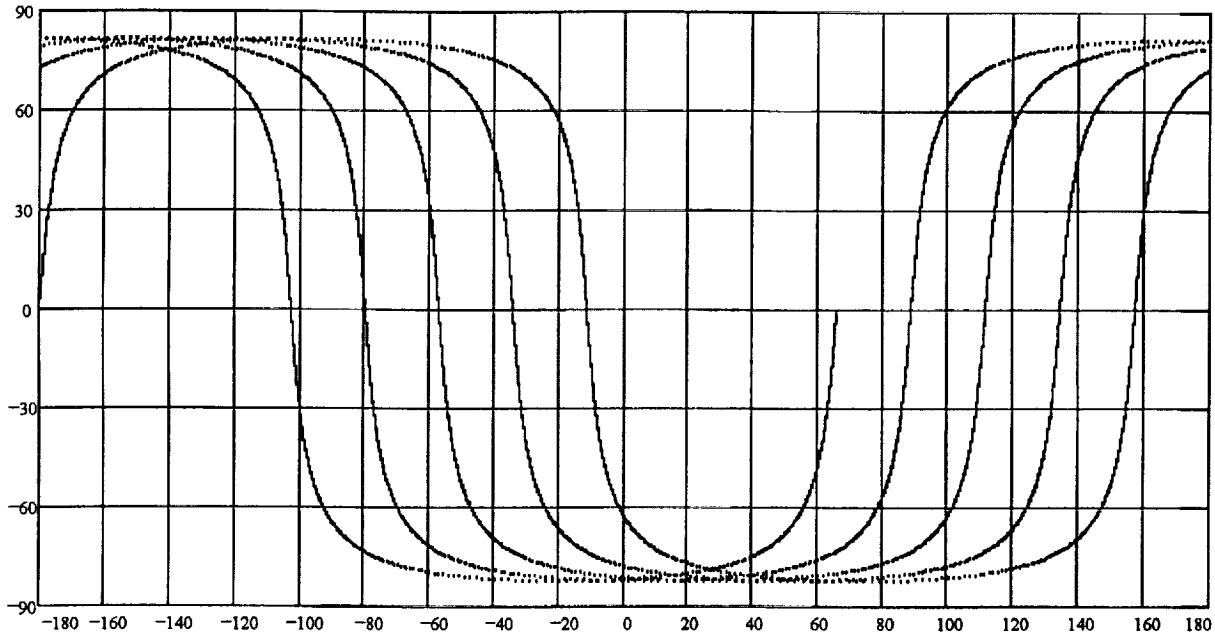

Plot latitude and longitude as a function of time

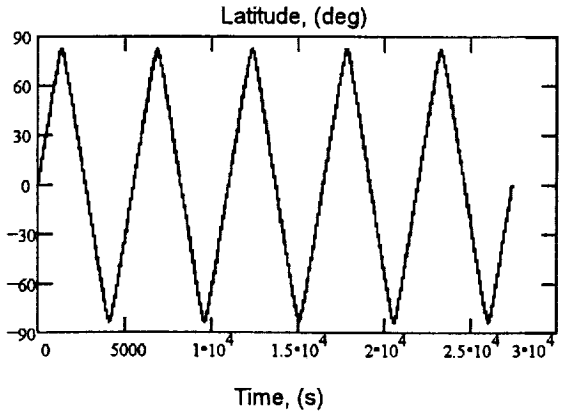

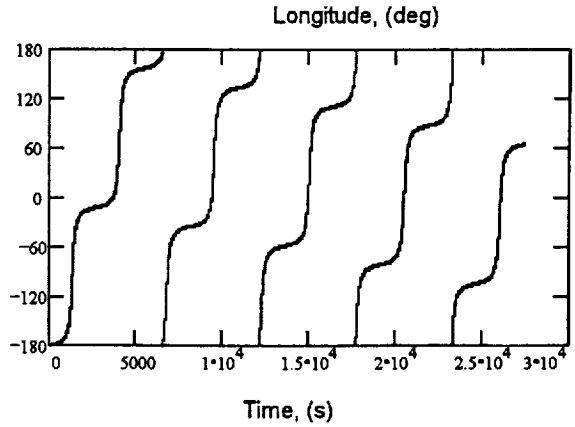

This portion calculates the angle that the orbit makes wrt to the lines of longitude. It does this by calculating the change in the latitude and longitude points between the current location and the previous location and uses simple geometry to calculate resultant angle using right spherical triangle geometry.

$$dlat_i := if(i>0, lat_i - lat_{i-1}, 0) \qquad dlong_i := if(i>0, long_i - long_{i-1}, 0) \qquad dangle_i := \left[\frac{atan\left(\frac{\tan(dlat_i)}{\sin(dlong_i)}\right)}{deg} \right]$$

Angle between orbit track and lines of longitude as a function of time.

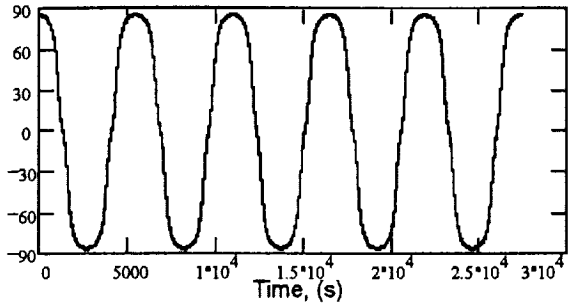

Angle between orbit track and lines of longitude as a function of latitude.

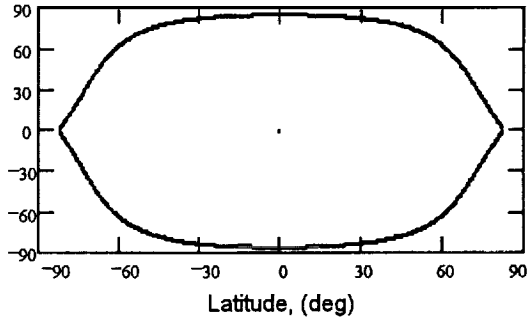

Angle between orbit track and lines of longitude as a function of longitude.

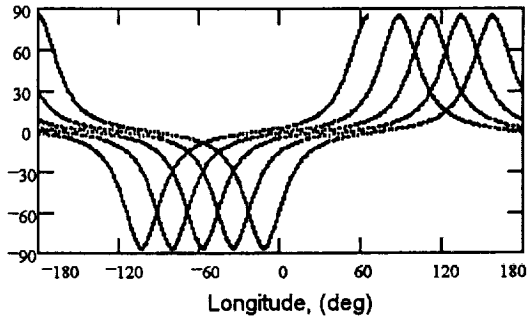

Appendix III Receiver Design Code

The following sections list the code of the receiver design model.

(IIIa) The optical page

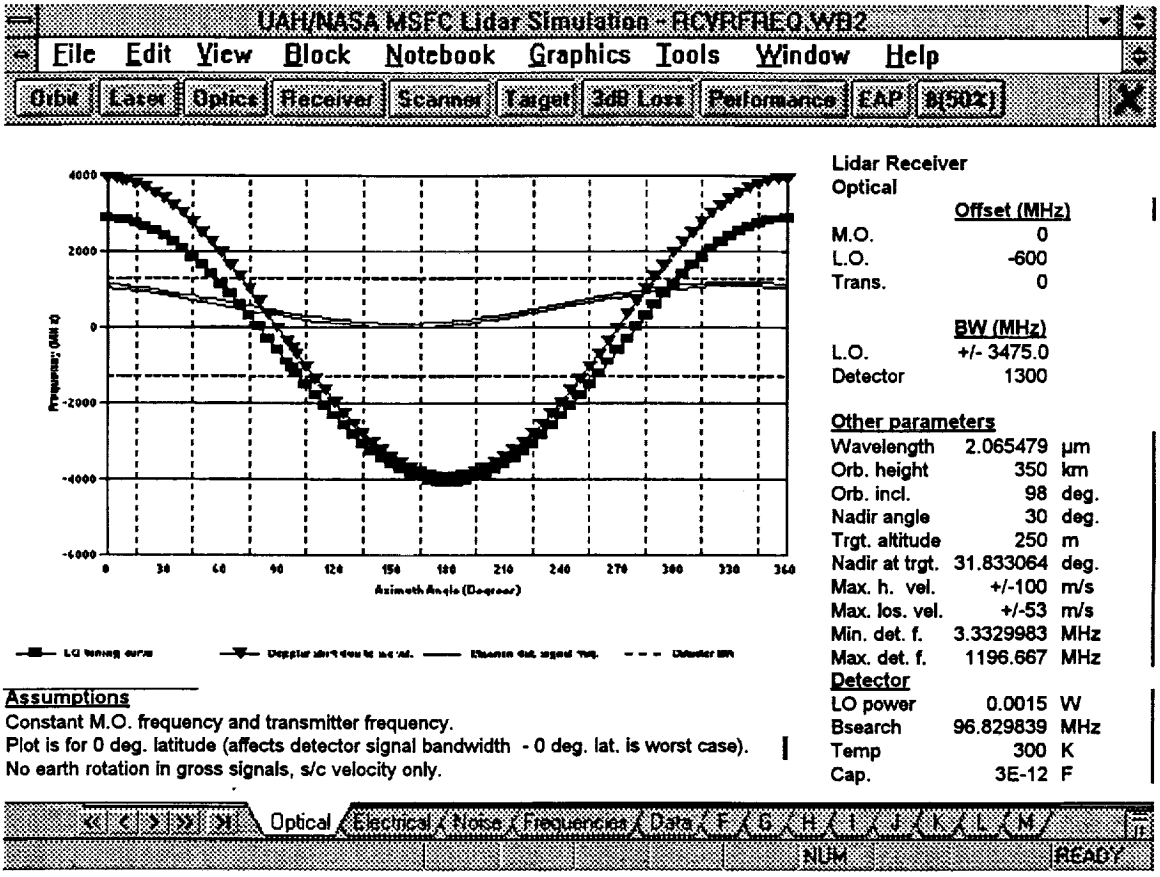

Figure (III-1) Visual appearance of the optical page.

The page shows (Figure (III-1)), as a function of azimuth angle, a plot of the Doppler shift due to the satellite velocity, the local oscillator tuning, the detector bandwidth and the residual frequency shifts due to the wind velocity and earth's rotational velocity. It also shows the major parameters of the model and a brief summary of the assumptions used for the plot. The graphical interface around the information is available on all the pages but for clarity will not be shown in future figures. The following listing provides the spreadsheet code embedded in the cells of the page.

```
Optical:J2:     'Lidar Receiver
Optical:J3:     'Optical
Optical:K4:     'Offset (MHz)
Optical:J5:     'M.O.
Optical:K5:     0
```

```
Optical:J6:    'L.O.
Optical:K6:    50
Optical:J7:    'Trans.
Optical:K7:    0
Optical:K9:    'BW (MHz)
Optical:J10:   'L.O.
Optical:K10:   0
Optical:J11:   'Detector
Optical:K11:   1250
Optical:J13:   'Other parameters
Optical:J14:   'Wavelength
Optical:K14:   +[LIDAR]LAMBDA
Optical:L14:   'um
Optical:J15:   'Orb. height
Optical:K15:   +[LIDAR]ORBH
Optical:L15:   'km
Optical:J16:   'Orb. incl.
Optical:K16:   +[LIDAR]ORBINC
Optical:L16:   'deg.
Optical:J17:   'Nadir angle
Optical:K17:   +[LIDAR]NADIR
Optical:L17:   'deg.
Optical:J18:   'Trgt. altitude
Optical:K18:   +[LIDAR]ALT
Optical:L18:   'm
Optical:J19:   'Nadir at trgt.
Optical:K19:   +[LIDAR]NADALT
Optical:L19:   'deg.
Optical:J20:   'Max. h.  vel.
Optical:K20:   100
Optical:L20:   'm/s
Optical:J21:   'Max. los. vel.
Optical:K21:   +K20*@SIN(@RADIANS(K19))
Optical:L21:   'm/s
Optical:J22:   'Min. det. f.
Optical:K22:   @MIN(F:L6..F:L81)
Optical:L22:   'MHz
Optical:J23:   'Max. det. f.
Optical:K23:   @MAX(F:K6..F:K81)
Optical:L23:   'MHz
Optical:J24:   'Detector
Optical:A25:   'Assumptions
Optical:J25:   'LO power
Optical:K25:   0.0006
Optical:L25:   'W
Optical:A26:   'Constant M.O. frequency and transmitter frequency.
Optical:J26:   'Bsearch
Optical:K26:   +$K20*2/[LIDAR]LAMBDA*10^6/1000000
Optical:L26:   'MHz
Optical:A27:   'Plot is for 0 deg. latitude (affects detector signal
bandwidth  - 0 deg. lat. is worst case).
Optical:J27:   'Temp
Optical:K27:   @IF(@INT(K14)=2,300,70)
Optical:L27:   'K
```

```
Optical:A28:    'No earth rotation in gross signals, s/c velocity only.
Optical:J28:    'Cap.
Optical:K28:    3E-12
Optical:L28:    'F
```

(IIIb) The electrical page

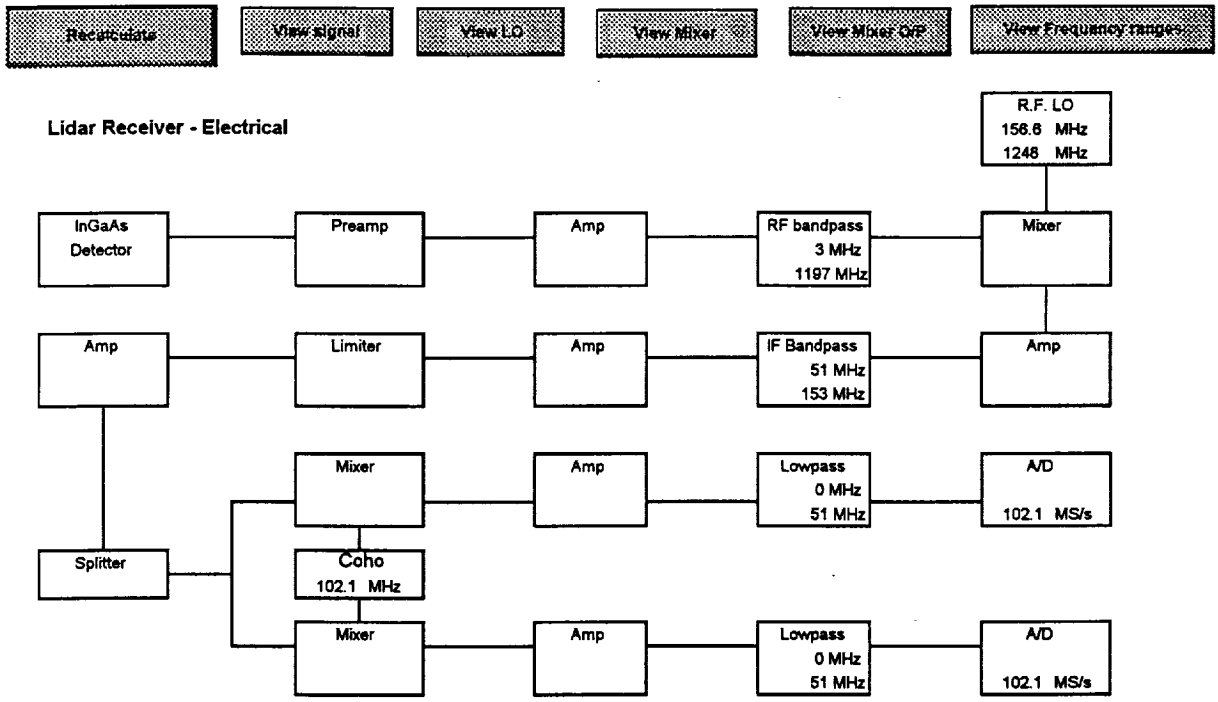

Figure (III-2) Visual appearance of the electrical page for a complex receiver design.

This page displays a block diagram (Figure (III-2) and Figure (III-3)) of the receiver electrical subsytem with critical frequencies at various points in the design. Thetop of the page contains a row of buttons, the first is used to run a macro (listed in Table (AIII.1)) to redraw the receiver design to match either a complex (Figure (III-2)) or real (Figure (III-3)) design depending on which the user has chosen. The remaining buttons are used to display a series of fullscreen plots which are summarised on a later page.

The top half of the block schematic is the same for both the complex and real receiver designs. The page simply contains a drawing for the bottom half of each of the receiver designs and hides/ unhides them according to the value of the complex receiver variable. The code on the page is listed below:

```
Electrical:M5:      '       R.F. LO
Electrical:B6:      'Lidar Receiver - Electrical
Electrical:M6:      @MIN(F:Q6..F:Q81)
Electrical:N6:      'MHz
```

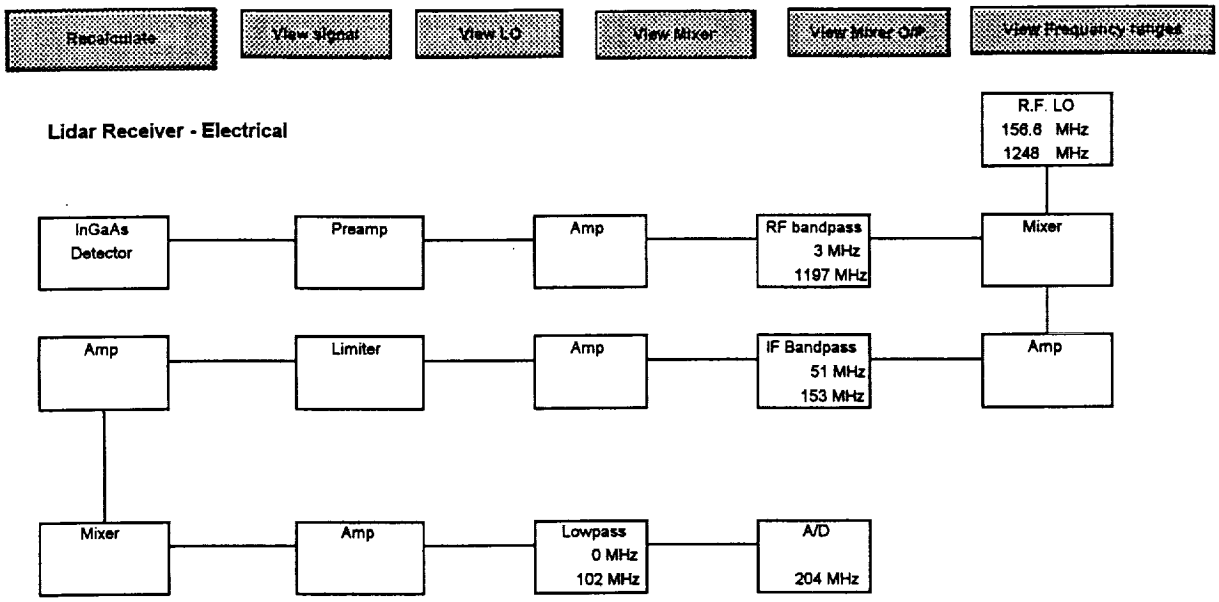

Figure (III-3) Visual appearance of the electrical page for a real receiver design.

```
Electrical:M7:    @MAX(F:Q6..F:Q81)
Electrical:N7:    'MHz
Electrical:B10:   @IF(@INT(Optical:K14)=2,"      InGaAs","      HgCdTe")
Electrical:F10:   '      Preamp
Electrical:I10:   '      Amp
Electrical:K10:   'RF bandpass
Electrical:M10:   '       Mixer
Electrical:T10:   'Lo
Electrical:U10:   'Hi
Electrical:B11:   "     Detector
Electrical:K11:   @IF(@MIN(F:L6..F:L81)<0,0,@MIN(F:L6..F:L81))
Electrical:S11:   'Signal
Electrical:T11:   +K11
Electrical:U11:   +K12
Electrical:K12:
@IF(@MAX(F:K6..F:K81)<@ABS(@MIN(F:L6..F:L81)),@ABS(@MIN(F:L6..F:L81)),@MAX(F:K
6..F:K81))
Electrical:S12:   'RF L.O.
Electrical:T12:   +M6
Electrical:U12:   +M7
Electrical:S13:   'I.F. Bandpass
Electrical:T13:   +K16
Electrical:U13:   +K17
Electrical:S14:   'A/D Lowpass
Electrical:T14:   +K21
Electrical:U14:   @IF([LIDAR]$rcvr_type="Complex",+K22,+I36)
Electrical:B15:   '        Amp
Electrical:F15:   '      Limiter
Electrical:I15:   '      Amp
Electrical:K15:   'IF Bandpass
```

```
Electrical:M15:    '         Amp
Electrical:K16:    @MIN(F:R6..F:R81,F:S6..F:S81)
Electrical:K17:    @MAX(F:R6..F:R81,F:S6..F:S81)
Electrical:F20:    '        Mixer
Electrical:I20:    '       Amp
Electrical:K20:    '    Lowpass
Electrical:M20:    '         A/D
Electrical:K21:    0
Electrical:K22:    +M22/2
Electrical:M22:    +Optical:K21*2/[LIDAR]$LAMBDA*2
Electrical:N22:    'MS/s
Electrical:B24:    '       Splitter
Electrical:F24:    '       Coho
Electrical:F25:    +M22
Electrical:G25:    'MHz
Electrical:F27:    '        Mixer
Electrical:I27:    '       Amp
Electrical:K27:    '    Lowpass
Electrical:M27:    '         A/D
Electrical:K28:    0
Electrical:K29:    +M29/2
Electrical:M29:    +Optical:K21*2/[LIDAR]$LAMBDA*2
Electrical:N29:    'MS/s
Electrical:B34:    '        Mixer
Electrical:F34:    '         Amp
Electrical:I34:    '     Lowpass
Electrical:K34:    '         A/D
Electrical:I35:    0
Electrical:I36:    +K36/2
Electrical:K36:    +Optical:K21*2/[LIDAR]Instrument:C8*4
```

	A	D
42	rcvr_pic_displa	{IF [lidar]$rcvr_type="Complex"}{BRANCH complex_rcvr}
43		{BRANCH real_rcvr}
44	complex_rcvr	{SETOBJECTPROPERTY "[RCVRFREQ]complex_pic.Reveal/ Hide","Rows,Reveal"}
45		{SETOBJECTPROPERTY "[RCVRFREQ]real_pic.Reveal/ Hide","Rows,Hide"}
46		{BRANCH done_rcvr}
47	real_rcvr	{SETOBJECTPROPERTY "[RCVRFREQ]complex_pic.Reveal/ Hide","Rows,Hide"}
48		{SETOBJECTPROPERTY "[RCVRFREQ]real_pic.Reveal/ Hide","Rows,Reveal"}
49	done_rcvr	{HOME}{RIGHT}{DOWN}

Table (III.1) The macro used to display the correct electrical block diagram.

(IIIc) The noise page

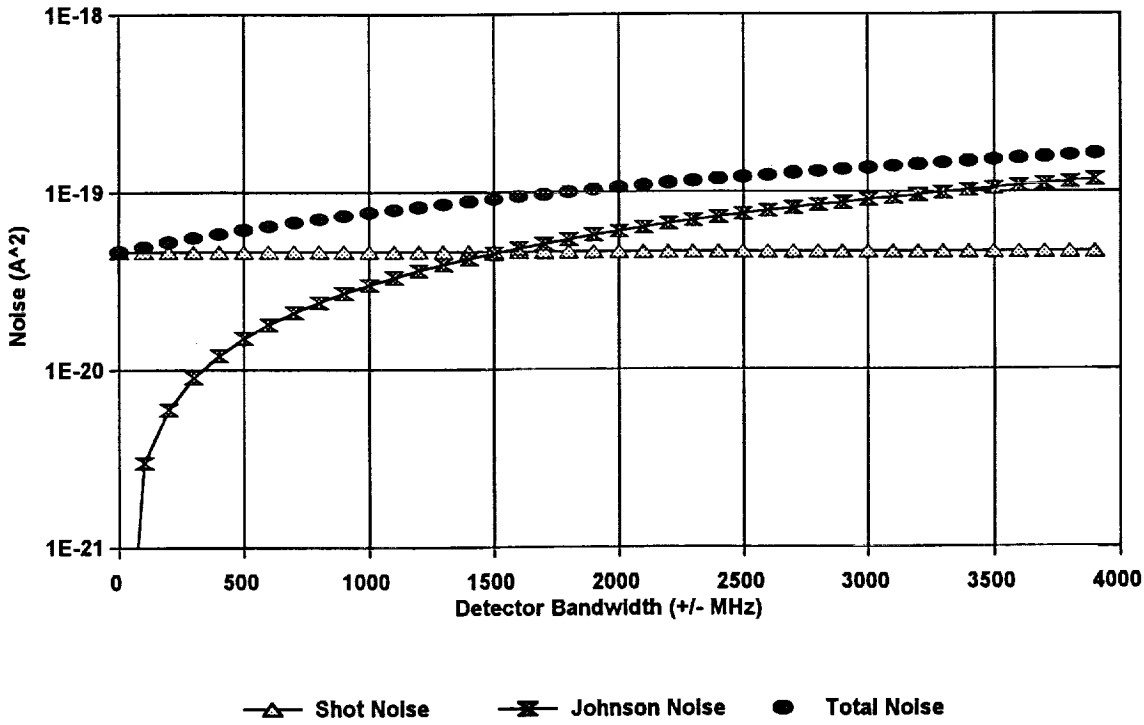

Figure (III-4) Visual appearance of the noise page.

This page simply displays the shot noise, Johnson noise and total noise as a function of the detector bandwidth required. The calculation is carried out using the following code:

```
Noise:D1:     'Noise
Noise:A2:     'Bdet
Noise:B2:     'Blo
Noise:C2:     'Shot
Noise:D2:     'Johnson
Noise:E2:     'Total
Noise:A3:     1
Noise:B3:     -(A3-$F:$G$6-Optical:$K$26*1E-06/2)
Noise:C3:     +2*[LIDAR]$e^2*[LIDAR]$QE*Optical:$K$25*Optical:$K$26/
([LIDAR]$H*[LIDAR]$FREQ*10^6)
Noise:D3:     +4*[LIDAR]$k*Optical:$K$27*Opti-
cal:$K$26*2*@PI*@ABS(A3*10^6)*Optical:$K$28
Noise:E3:     +C3+D3
Noise:A4:     100
Noise:B4:     -(A4-$F:$G$6-Optical:$K$26*1E-06/2)
Noise:C4:     +2*[LIDAR]$e^2*[LIDAR]$QE*Optical:$K$25*Optical:$K$26/([LIDAR]$H
                  +2*[LIDAR]$e^2*[LIDAR]$QE*Optical:$K$25*Optical:$K$26/
([LIDAR]$H*[LIDAR]$FREQ*10^6)
```

```
Noise:D4:     +4*[LIDAR]$k*Optical:$K$27*Opti-
cal:$K$26*2*@PI*@ABS(A4*10^6)*Optical:$K$28
Noise:E4:     +C4+D4
```

Each succsive row repeats, incrementing the detector bandwidth until the final row is reached.

```
Noise:A42:    3900
Noise:B42:    -(A42-$F:$G$6-Optical:$K$26*1E-06/2)
Noise:C42:    +2*[LIDAR]$e^2*[LIDAR]$QE*Optical:$K$25*Optical:$K$26/
([LIDAR]$H*[LIDAR]$FREQ*10^6)
Noise:D42:    +4*[LIDAR]$k*Optical:$K$27*Opti-
cal:$K$26*2*@PI*@ABS(A42*10^6)*Optical:$K$28
Noise:E42:    +C42+D42
```

(IIId) The frequencies page

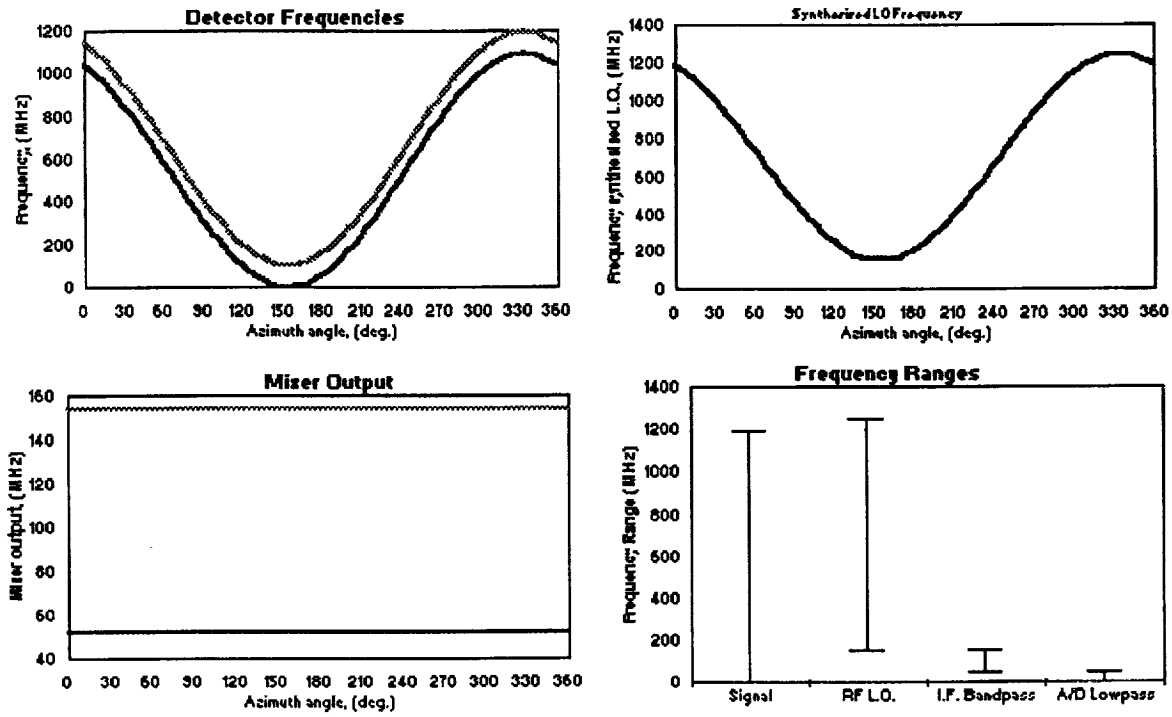

Figure (III-5) Visual appearance of the frequency page.

This page simply displays multiple small graphs showing the frequency at various points in the receiver design.

(IIIe) The data rate calculation page

This page displays the A/D speed and data storage requirements. The code is listed below:

Wavelength	2.065479	µm						
Max. horizontal velocity	100	m/s						
Max. line of sight velocity (occurs at ground)	52.7466857	m/s						
Max. nadir error (any direction)	+/- 0.1	deg.						
Worst case line of sight velocity shift due to nadir error	12.4379616	m/s						
Max line of sight velocity allowing for nadir error	65.1846473	m/s						
Velocity bandwidth required to this point	130.369295	m/s						
Signal bandwidth required to this point	126.236379	MHz						
XMTR/LO frequency offset error	+/- 5	MHz						
Additional bandwidth to account for XMTR/LO offset error	10	MHz						
Total bandwidth required	136.236379	MHz						
Real/Complex receiver geometry	Complex							
Sampling rate over Nyquist	1.1	(1 = Nyquist, 2 = Twice as many samples as Nyquist etc.)						
Sampling rate required/ channel	149.860017	Msamples/s						
No. bits	12	bits/sample						
pk. bits/s (one channel)	1.7983E+09	bits/s						
pk. bits/s (all channels)	3.5966E+09	bits/s		No Error		With Error		
Max altitude	15	km	nadir	31.7509	deg.	31.85814	de	
Min altitude	0	km	nadir	31.8345	deg.	31.942	de	
slant range margin	1	km						
slant range	18.6478888	km						
digitisation time	124.405323	µs						
bits/pulse	447442	bits/pulse						
ancillary words/ pulse	20	words/pulse						
total bits/pulse	447682	bits/pulse						
PRF	20	Hz						
Bits/s averaged over one second	8953640	bits/s						
Orbit duration	5481.50413	s						
Data storage	4.9079E+10	bits/orbit						

Figure (III-6) Visual appearance of the data requirements page.

```
Data:A1:    Wavelength
Data:B1:    +Optical:K14
Data:C1:    'um
Data:A2:    Max. horizontal velocity
Data:B2:    100
Data:C2:    m/s
Data:A3:    Max. line of sight velocity (occurs at ground)
Data:B3:    +B2*@SIN(@RADIANS(E19))
Data:C3:    m/s
Data:A4:    Max. nadir error (any direction)
Data:B4:    0.1
Data:C4:    deg.
Data:A5:    Worst case line of sight velocity shift due to nadir error
Data:B5:    @ABS((B2+[LIDAR]$VSAT)*(@SIN(@RADIANS(G19))-@SIN(@RADIANS(E19))))
Data:C5:    m/s
Data:A6:    Max line of sight velocity allowing for nadir error
Data:B6:    +B3+B5
Data:C6:    m/s
Data:A7:    Velocity bandwidth required to this point
Data:B7:    +B6*2
Data:C7:    m/s
Data:A8:    Signal bandwidth required to this point
Data:B8:    +B7*2/(B1)
Data:C8:    MHz
Data:A9:    XMTR/LO frequency offset error
Data:B9:    5
```

```
Data:C9:    MHz
Data:A10:   Additional bandwidth to account for XMTR/LO offset error
Data:B10:   +B9*2
Data:C10:   MHz
Data:A11:   Total bandwidth required
Data:B11:   +B8+B10
Data:C11:   MHz
Data:A12:   Real/Complex receiver geometry
Data:B12:   +[LIDAR]rcvr_type
Data:A13:   Sampling rate over Nyquist
Data:B13:   1.1
Data:C13:   '(1 = Nyquist, 2 = Twice as many samples as Nyquist etc.)
Data:A14:   Sampling rate required/ channel
Data:B14:   @IF(B12="Complex",+B11*B13,+B11*B13*2)
Data:C14:   Msamples/s
Data:A15:   No. bits
Data:B15:   12
Data:C15:   bits/sample
Data:A16:   pk. bits/s (one channel)
Data:B16:   +B15*B14*10^6
Data:C16:   bits/s
Data:A17:   pk. bits/s (all channels)
Data:B17:   (@IF(B12="Complex",2,1))*B16
Data:C17:   bits/s
Data:E17:   No Error
Data:G17:   With Error
Data:A18:   Max altitude
Data:B18:   15
Data:C18:   km
Data:D18:   nadir
Data:E18:   @DEGREES(@ASIN(([LIDAR]$ORBH*10^3+[LIDAR]$RE)*@SIN(@RADI-
ANS([LIDAR]$NADIR))/([LIDAR]$RE+B18*1000)))
Data:F18:   deg.
Data:G18:   @DEGREES(@ASIN(([LIDAR]$ORBH*10^3+[LIDAR]$RE)*@SIN(@RADI-
ANS([LIDAR]$NADIR+B4))/([LIDAR]$RE+B18*1000)))
Data:H18:   deg.
Data:A19:   Min altitude
Data:B19:   0
Data:C19:   km
Data:D19:   nadir
Data:E19:   @DEGREES(@ASIN(([LIDAR]$ORBH*10^3+[LIDAR]$RE)*@SIN(@RADI-
ANS([LIDAR]$NADIR))/([LIDAR]$RE+B19*1000)))
Data:F19:   deg.
Data:G19:   @DEGREES(@ASIN(([LIDAR]$ORBH*10^3+[LIDAR]$RE)*@SIN(@RADI-
ANS([LIDAR]$NADIR+B4))/([LIDAR]$RE+D19*1000)))
Data:H19:   deg.
Data:A20:   slant range margin
Data:B20:   1
Data:C20:   km
Data:A21:   slant range
Data:B21:   +B20+@SQRT((+B18*10^3+[LIDAR]$RE)^2+([LIDAR]$RE)^2-
(2*B18*10^3+2*[LIDAR]$RE)*([LIDAR]$RE)*@COS(@RADIANS(E19-E18)))/1000
Data:C21:   km
Data:A22:   digitisation time
```

```
Data:B22:   (2*B21*1000)/[LIDAR]$C/10^-6
Data:C22:   'us
Data:A23:   bits/pulse
Data:B23:   @CEILING(B17*B22/10^6,1)
Data:C23:   bits/pulse
Data:A24:   ancillary words/ pulse
Data:B24:   20
Data:C24:   words/pulse
Data:A25:   total bits/pulse
Data:B25:   +B23+(B24*B15)
Data:C25:   bits/pulse
Data:A26:   PRF
Data:B26:   +[LIDAR]$PRF
Data:C26:   Hz
Data:A27:   Bits/s averaged over one second
Data:B27:   +B25*B26
Data:C27:   bits/s
Data:A29:   Orbit duration
Data:B29:   +[LIDAR]$TORBIT
Data:C29:   s
Data:A30:   Data storage
Data:B30:   +B29*B27
Data:C30:   bits/orbit
Data:B31:   +B30/B15
Data:C31:   words/orbit
```

(IIIf) The calculation page

	<----------			----------	----------	----------	----------OPTICAL PORTION OF RECEIVER----------				----------	----------	---------->	
							Frequency shift (MHz) due to:							
Telescope	Laser frequency offsets			Laser frequency diffs.		Sat. Velocity	Earth rotn.	Sat. +earth. ± wind		Residual after LO		detector BW		Detector f
Azimuth		(MHz			(MHz)			dVs+dVe	dVs+dVe	(sig. on electronics)		(MHz)		(MHz)
(deg)	M.O.	Tx	L.O.	M.O.-Tx	M.O.-L.O.	dVs	dVe	+Vmax	-Vmax	max	min	det+	det-	max
0	0	0	50	0	-50	3934.791457	32.933543	4018.798	3916.652	3968.798	3866.652	1250	-1250	3968.798
5	0	0	50	0	-50	3919.818388	12.384638	3983.276	3881.13	3933.276	3831.13	1250	-1250	3933.276
8	0	0	50	0	-50	3896.498337	0	3947.571	3845.426	3897.571	3795.426	1250	-1250	3897.571
345	0	0	50	0	-50	3800.716689	92.461549	3944.251	3842.106	3894.251	3792.106	1250	-1250	3894.251
350	0	0	50	0	-50	3875.013133	73.124939	3999.211	3897.066	3949.211	3847.066	1250	-1250	3949.211
355	0	0	50	0	-50	3919.818388	53.231804	4024.123	3921.978	3974.123	3871.978	1250	-1250	3974.123
360	0	0	50	0	-50	3934.791457	32.933543	4018.798	3916.652	3968.798	3866.652	1250	-1250	3968.798

Figure (III-7) Visual appearance of the calculation page.

This page contains the code to calculate the local oscillator frequency offsets. It is not intended to be part of the user interface, although it is accessible to the user. Figure (III-7) shows the top and bottom of the page and the code is listed below:

```
F:B1:     '<--------------------
F:D1:     '--------------------
F:E1:     '--------------------
F:F1:     '--------------------
F:G1:     '----------------------
F:H1:     '----------OPTICAL PORTION OF RECEIVER
```

```
F:L1:     '---------------
F:M1:     '----------------------
F:N1:     '--------->
F:H2:     'Frequency shift (MHz) due to:
F:A3:     ^Telescope
F:B3:     'Laser frequency offsets
F:E3:     'Laser frequency diffs.
F:G3:     'Sat. Velocity
F:H3:     'Earth rotn.
F:I3:     'Sat. +earth. + wind
F:K3:     'Residual after LO
F:M3:     'detector BW
F:O3:     'Detector frequencies
F:Q3:     ^Mixer
F:R3:     "Output from
F:A4:     ^Azimuth
F:C4:     '(MHz)
F:F4:     '(MHz)
F:I4:     'dVs+dVe
F:J4:     'dVs+dVe
F:K4:     '(sig. on electronics)
F:M4:     "(MHz)
F:O4:     "(MHz)
F:Q4:     ^Frequency
F:R4:     "Mixer
F:A5:     ^(deg)
F:B5:     ^M.O.
F:C5:     ^Tx
F:D5:     ^L.O.
F:E5:     ^M.O.-Tx
F:F5:     ^M.O.-L.O.
F:G5:     ^dVs
F:H5:     'dVe
F:I5:     "+Vmax
F:J5:     "-Vmax
F:K5:     'max
F:L5:     'min
F:M5:     'det+
F:N5:     'det-
F:O5:     'max
F:P5:     'min
F:Q5:     ^(MHz)
F:R5:     "(MHz)
F:A6:     0
F:B6:     +Optical:$K$5
F:C6:     +B6+$Optical:$K$7
F:D6:     +$Optical:$K$6+$Optical:$K$10*@COS(@RADIANS(A6))
F:E6:     +B6-C6
F:F6:     +B6-D6
F:G6:     +[LIDAR]$VSAT*2/[LIDAR]$LAMBDA*@SIN(@RADIANS([LIDAR]$NAD-
ALT))*@COS(@RADIANS(A6))
F:H6:     +2*[LIDAR]$VEARTH*@SIN(@RADIANS(8-A6))*@SIN(@RADIANS([LIDAR]$NAD-
ALT))/[LIDAR]$LAMBDA
```

```
F:I6:     +$G6+$H6+2*Optical:$K$20*@SIN(@RADIANS([LIDAR]$NADALT))/
[LIDAR]$LAMBDA
F:J6:     +$G6+$H6-2*Optical:$K$20*@SIN(@RADIANS([LIDAR]$NADALT))/
[LIDAR]$LAMBDA
F:K6:     +I6+F6
F:L6:     +J6+F6
F:M6:     +$Optical:$K$11
F:N6:     -$Optical:$K$11
F:O6:     @ABS(K6)
F:P6:     @ABS(L6)
F:Q6:     (O6+P6)/2+Electrical:$F$25
F:R6:     @ABS(Q6-O6)
F:S6:     @ABS(Q6-P6)
F:A7:     5
F:B7:     +Optical:$K$5
F:C7:     +B7+$Optical:$K$7
F:D7:     +$Optical:$K$6+$Optical:$K$10*@COS(@RADIANS(A7))
F:E7:     +B7-C7
F:F7:     +B7-D7
F:G7:     +[LIDAR]$VSAT*2/[LIDAR]$LAMBDA*@SIN(@RADIANS([LIDAR]$NAD-
ALT))*@COS(@RADIANS(A7))
F:H7:     +2*[LIDAR]$VEARTH*@SIN(@RADIANS(8-A7))*@SIN(@RADIANS([LIDAR]$NAD-
ALT))/[LIDAR]$LAMBDA
F:I7:     +$G7+$H7+2*Optical:$K$20*@SIN(@RADIANS([LIDAR]$NADALT))/
[LIDAR]$LAMBDA
F:J7:     +$G7+$H7-2*Optical:$K$20*@SIN(@RADIANS([LIDAR]$NADALT))/
[LIDAR]$LAMBDA
F:K7:     +I7+F7
F:L7:     +J7+F7
F:M7:     +$Optical:$K$11
F:N7:     -$Optical:$K$11
F:O7:     @ABS(K7)
F:P7:     @ABS(L7)
F:Q7:     (O7+P7)/2+Electrical:$F$25
F:R7:     @ABS(Q7-O7)
F:S7:     @ABS(Q7-P7)
```

The code repeats on successive rows, incrementing the azimuth each time. Finally the end of the table is reached:

```
F:A81:    360
F:B81:    +Optical:$K$5
F:C81:    +B81+$Optical:$K$7
F:D81:    +$Optical:$K$6+$Optical:$K$10*@COS(@RADIANS(A81))
F:E81:    +B81-C81
F:F81:    +B81-D81
F:G81:    +[LIDAR]$VSAT*2/[LIDAR]$LAMBDA*@SIN(@RADIANS([LIDAR]$NAD-
ALT))*@COS(@RADIANS(A81))
F:H81:    +2*[LIDAR]$VEARTH*@SIN(@RADIANS(8-A81))*@SIN(@RADIANS([LIDAR]$NAD-
ALT))/[LIDAR]$LAMBDA
F:I81:    +$G81+$H81+2*Optical:$K$20*@SIN(@RADIANS([LIDAR]$NADALT))/
[LIDAR]$LAMBDA
F:J81:    +$G81+$H81-2*Optical:$K$20*@SIN(@RADIANS([LIDAR]$NADALT))/
[LIDAR]$LAMBDA
```

```
F:K81:    +I81+F81
F:L81:    +J81+F81
F:M81:    +$Optical:$K$11
F:N81:    -$Optical:$K$11
F:O81:    @ABS(K81)
F:P81:    @ABS(L81)
F:Q81:    (O81+P81)/2+Electrical:$F$25
F:R81:    @ABS(Q81-O81)
F:S81:    @ABS(Q81-P81)
```

Appendix IV AEOLUS Power Budget on Free Flyer Spacecraft

The enclosed plots show the average power requirements for a 0.4 J CO_2 AEOLUS instrument with a dual-look fixed telescope arrangement mounted on a generic spacecraft. A 350 km, 98 degree orbit was assumed and the worst case orbit (maximum time in the shade) was considered. Three different power management schemes have been considered:-

A) The laser is operated at a constant 20 Hz PRF for 5% of the orbit during the shade portion of the orbit.

B) The laser is operated at a constant 20 Hz PRF for 5% of the orbit during the sun portion of the orbit.

C) The laser is not turned on during the orbit.

For each shot management scheme the following parameters were plotted as a function of time:

Power:- This shows the average power requirements over one scan. The power requirement calculated is for the total spacecraft system, not just the AEOLUS instrument.

Battery capacity:- This shows the charge remaining in the batteries as a function of time / latitude.

During the non-operational period of the orbit, it is assumed that all systems are operational and only the laser pulsing is turned off. The instrument is composed of several sub-systems which are powered continuously. The power for each of these sub-systems was provided by Steve Johnson, MSFC EB-54,and are listed inTable IV.1).

Sub-system	Power (W)
Thermal control system	142
Laser	80
Receiver	60
Power conversion and distribution	50
Data acquisition and control	22
Lidar control	15
Wiring Harness (1 % of power distributed).	4

Table (IV.1) Instrument Standby Power Requirements

Sub-system	Power (W)
Total	373

Table (IV.1) Instrument Standby Power Requirements

During operation the laser sub-system requires an additional 236 W and the wiring harness power loss is increased to 6 W. The remaining parameters used in the model are listed in Table IV.2).

Power required by satellite	150 W
Solar array power generation	800 W
Solar cell losses (account for deterioration over mission life)	5% of total solar pwr.
Number of batteries on spacecraft	1
Storage capacity (single battery)	40 A-hr
Discharge depth allowed on batteries (fraction of maximum capacity)	0.7
Maximum charging rate of batteries (fraction of max. cap./hr.)	0.5
Efficiency of charging battery	0.866
Efficiency of battery discharge	0.866
LAWS laser PRF	20 Hz
LAWS laser duty cycle over one orbit	5%
Satellite speed	7.6059 $km.s^{-1}$
Orbit height	350 km
Orbit occultation occurs above	49 degrees
Average earth radius	6371.315 km

Table (IV.2) Parameters for a 9 μm AEOLUS on a Freeflyer Spacecraft.

Figure (AIV-1)shows the variation in latitude as a function of time for the orbit considered.

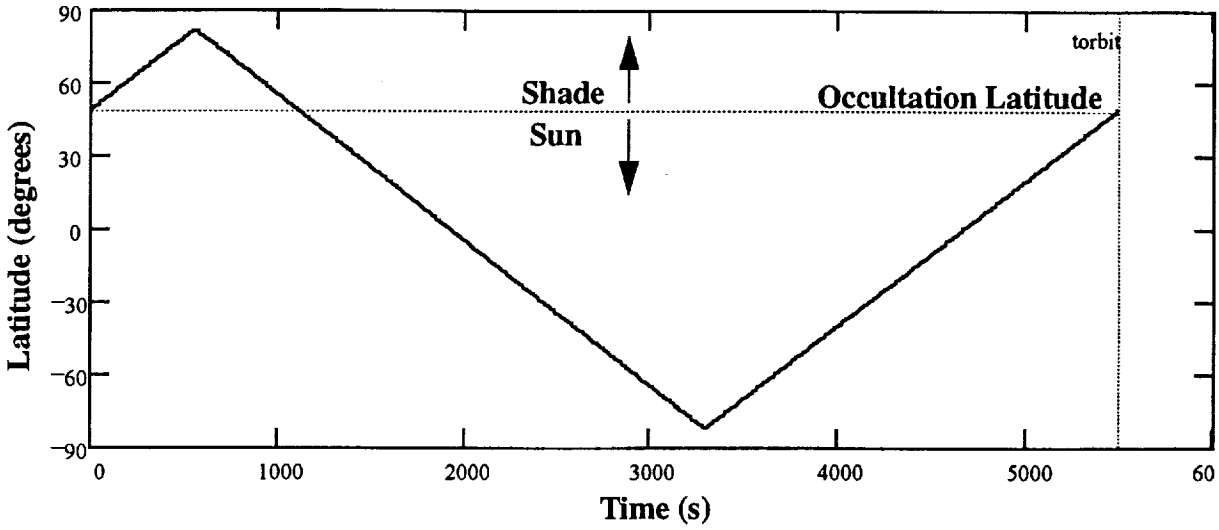

Figure (IV-1) Variation of latitude with time over one orbit.

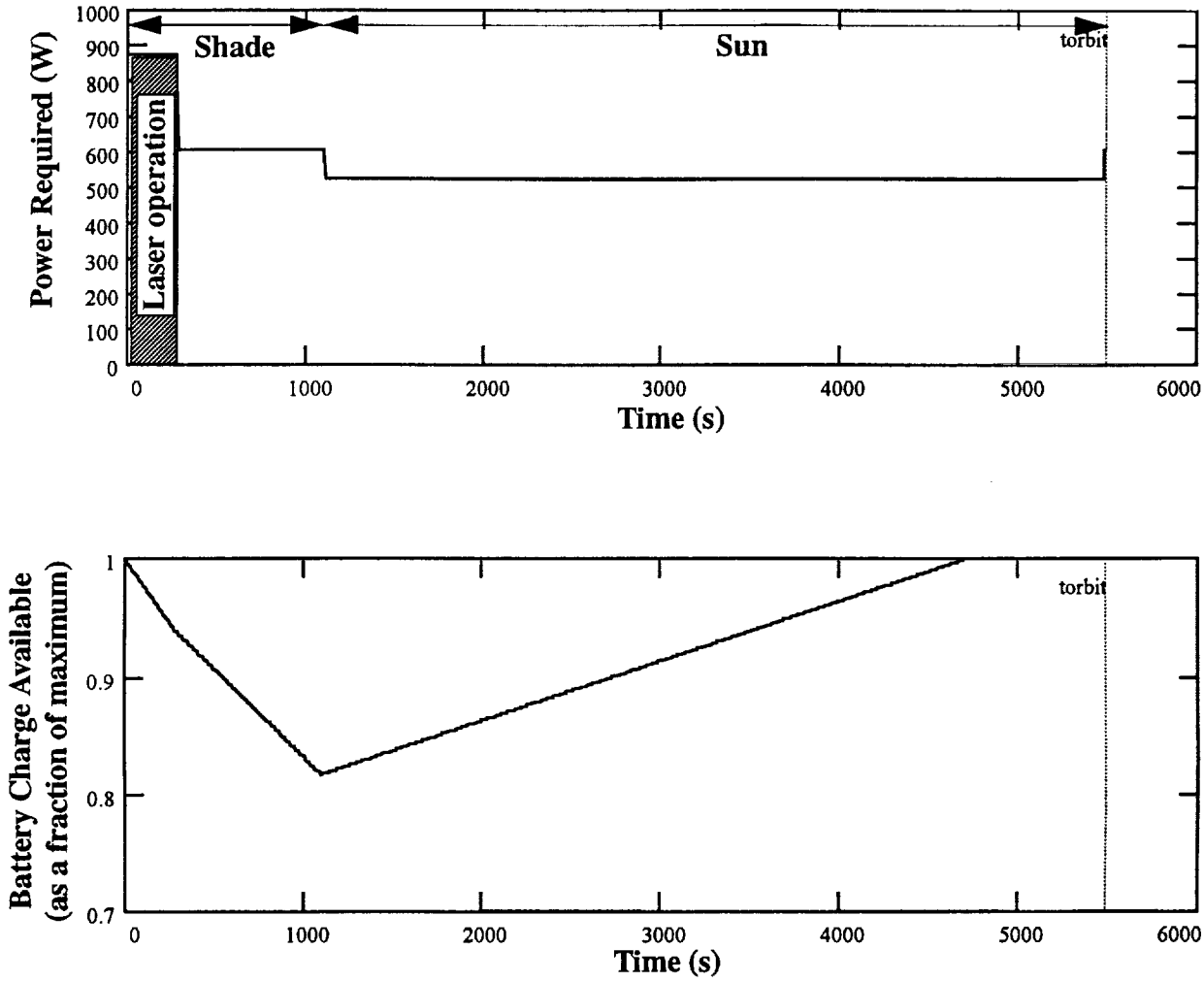

Figure (IV-2) The total power consumption and battery charging histories for one orbit when the laser is pulsed during the shade portion of the orbit.

From Figure (AIV-2) it can be seen that the batteries on the spacecraft are fully recharged before the orbit is over. The period from completion of recharging the batteries to the end of the orbit period represents a period when the power available from the solar arrays is not fully utilised. The energy 'lost' during this period can be divided by the total orbit time to give an average spare power capacity of the solar arrays. This spare capacity is ~ 28 W for this scenario. It can be seen that the transition from shade to sun results in a reduction of the power required. This is due to the elimination of the inefficiency of operating from the batteries.

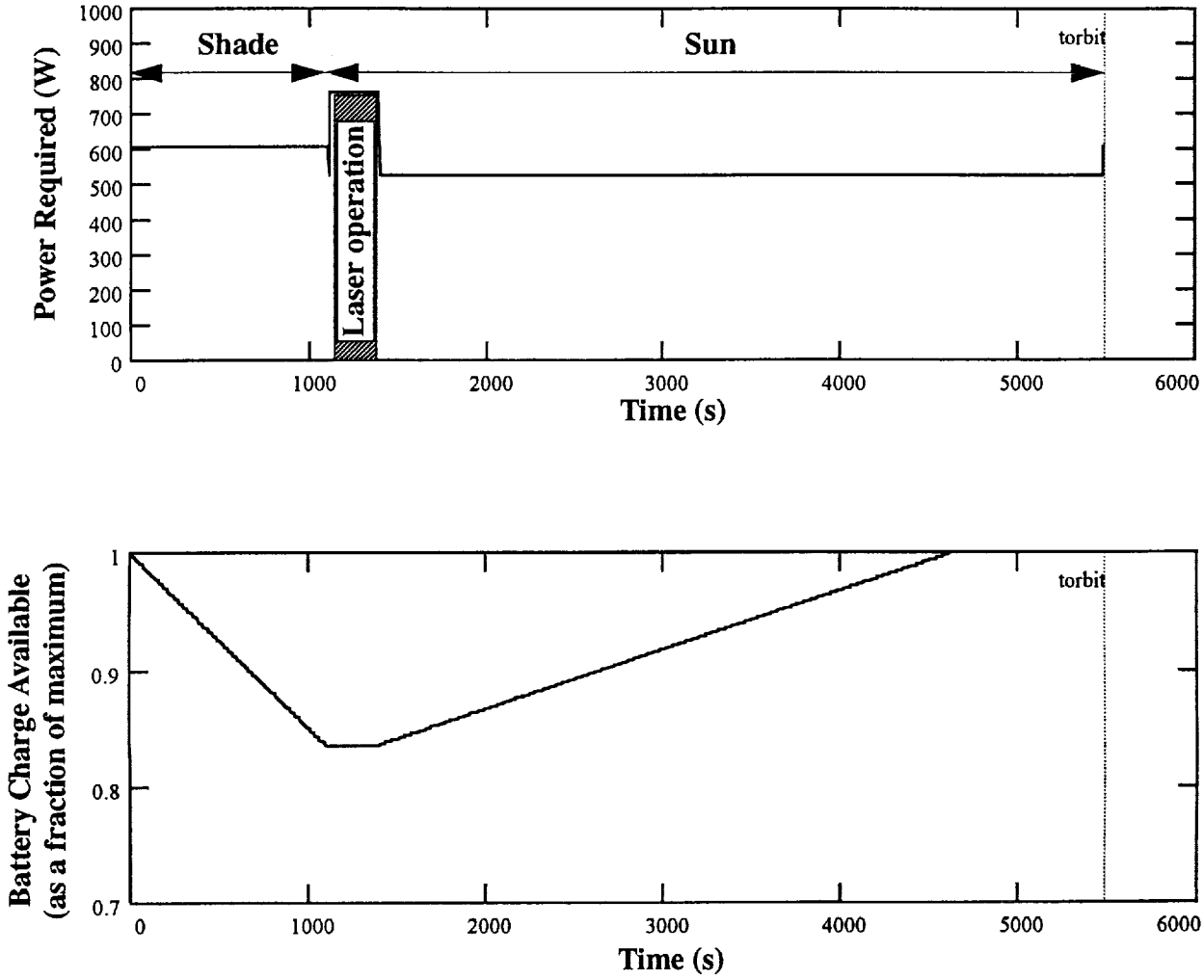

Figure (IV-3) The total power consumption and battery charging histories for one orbit when the laser is pulsed during the sun portion of the orbit.

From Figure (AIV-3) it can be seen that the batteries on the spacecraft are fully recharged before the orbit is over. The spare capacity is ~ 31 W for this scenario.

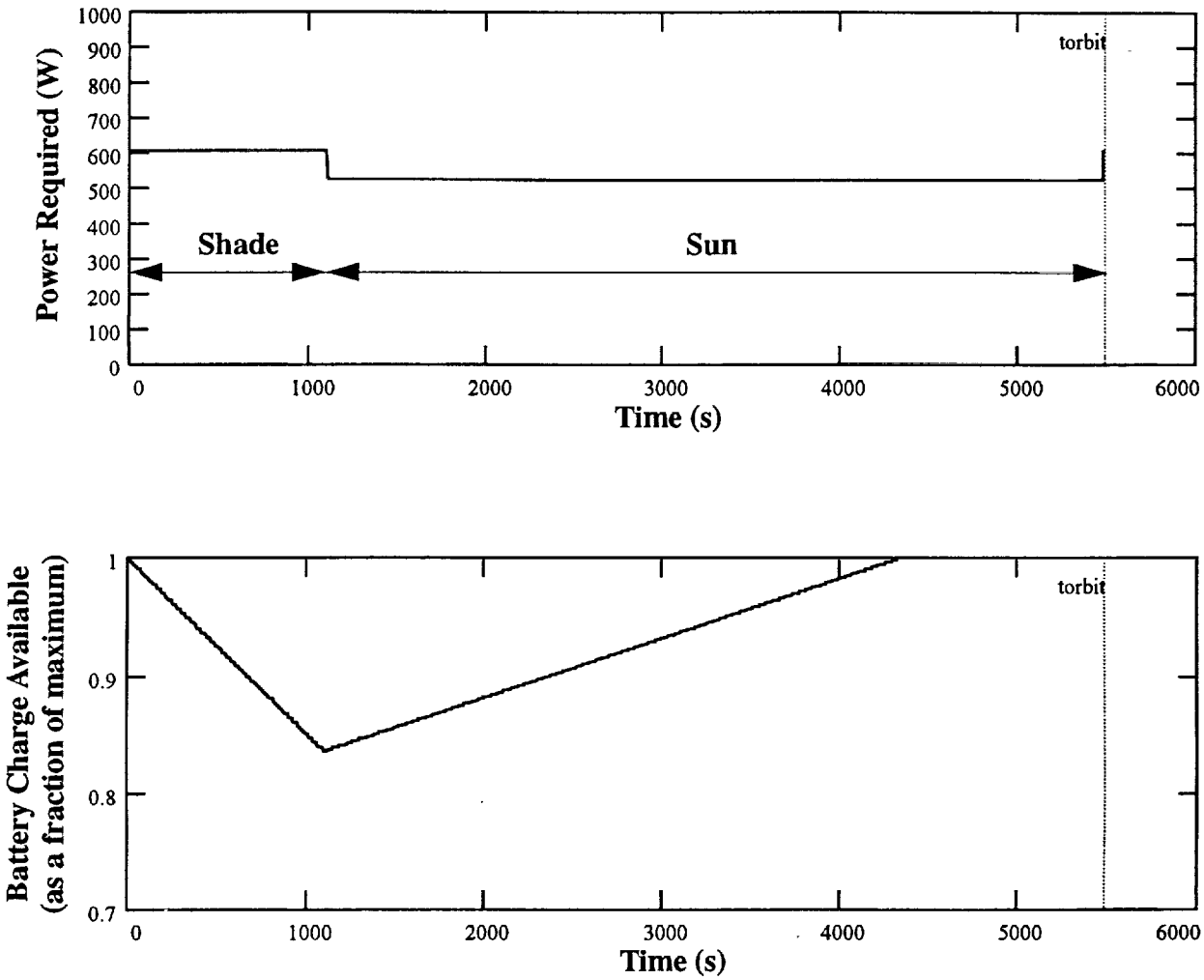

Figure (IV-4) The total power consumption and battery charging histories for one orbit when the laser is not pulsed over the whole orbit.

From Figure (AIV-4) it can be seen that the batteries on the spacecraft are fully recharged before the orbit is over. The spare capacity is ~ 42 W for this scenario.

(IVa) Conclusions

The difference between no laser operation and worst case operation (pulse during the shade) is ~ 14 W averaged over one orbit and thus it can be concluded from this analysis that the standby power requirement is the driver for an instrument of this design. Careful consideration of which sub-systems could be turned-off or placed in a reduced power consumption mode during the peri-

ods when the laser is not operational could result in a considerable power saving. Conversely increasing the duty cycle of the laser would result in a minimal increase in the solar power required for the current design.

National Aeronautical and Space Agency

Report Document Page

1. Report No.	2. Government Accession No.	3. Recipient's Catalog No.

4. Title and Subtitle

ANALYSES OF COHERENT LIDAR WIND MEASUREMENT MISSIONS

5. Report Due

November, 1995

6. Performing Organization Code

University of Alabama in Huntsville

7. Aurthor(s)

Gary D. Spiers

8. Performing Organization Report No.

10. Work Unit No.

9. Performing Organization Name and Address

University of Alabama in Huntsville
Huntsville, Alabama 35899

11. Contract or Grant No.

NAS8-38609, DO 128

12. Sponsoring Agency Name and Address

National Aeronautics and Space Administration
Washington, D.C. 20546-001
Marshall Space Flight Center, AL 35812

13. Type of report and Period covered

Final 11/2/94--11/1/95

14. Sponsoring Agency Code

15. Supplementary Notes

16.Abstract

17. Key Words (Suggested by Author(s))	18. Distribution Statement

19. Security Class. (of this report)	20. Security Class. (of this page)	21. No. of pages	22. Price
Unclassified	Unclassified		

NASA FORM 1626 OCT 86